

AD \_\_\_\_\_

Award Number: DAMD17-01-1-0326

TITLE: Automated Method for Analysis of Mammographic Breast  
Density - A Technique for Breast Cancer Risk Estimation

PRINCIPAL INVESTIGATOR: Heang Ping Chan, Ph.D.

CONTRACTING ORGANIZATION: University of Michigan  
Ann Arbor, Michigan 48109-1274

REPORT DATE: July 2002

TYPE OF REPORT: Annual

PREPARED FOR: U.S. Army Medical Research and Materiel Command  
Fort Detrick, Maryland 21702-5012

DISTRIBUTION STATEMENT: Approved for Public Release;  
Distribution Unlimited

The views, opinions and/or findings contained in this report are those of the author(s) and should not be construed as an official Department of the Army position, policy or decision unless so designated by other documentation.

120 075

# REPORT DOCUMENTATION PAGE

Form Approved  
OMB No. 074-0188

Public reporting burden for this collection of information is estimated to average 1 hour per response, including the time for reviewing instructions, searching existing data sources, gathering and maintaining the data needed, and completing and reviewing this collection of information. Send comments regarding this burden estimate or any other aspect of this collection of information, including suggestions for reducing this burden to Washington Headquarters Services, Directorate for Information Operations and Reports, 1215 Jefferson Davis Highway, Suite 1204, Arlington, VA 22202-4302, and to the Office of Management and Budget, Paperwork Reduction Project (0704-0188), Washington, DC 20503

|                                  |                             |   |
|----------------------------------|-----------------------------|---|
| 1. AGENCY USE ONLY (Leave blank) | 2. REPORT DATE<br>July 2002 | 3. REPORT TYPE AND DATES COVERED<br>Annual (1 Jul 01 - 30 Jun 02) |
|----------------------------------|-----------------------------|---|

|   |  |
|---|--|
| 4. TITLE AND SUBTITLE<br>Automated Method for Analysis of Mammographic Breast Density - A Technique for Breast Cancer Risk Estimation | 5. FUNDING NUMBERS<br>DAMD17-01-1-0326 |
|---|--|

|  |
|--|
| 6. AUTHOR(S)<br>Heang Ping Chan, Ph.D. |
|--|

|  |  |
|--|--|
| 7. PERFORMING ORGANIZATION NAME(S) AND ADDRESS(ES)<br>University of Michigan<br>Ann Arbor, Michigan 48109-1274<br><br>E-Mail: chanhp@umich.edu | 8. PERFORMING ORGANIZATION REPORT NUMBER |
|--|--|

|   |  |
|---|--|
| 9. SPONSORING / MONITORING AGENCY NAME(S) AND ADDRESS(ES)<br>U.S. Army Medical Research and Materiel Command<br>Fort Detrick, Maryland 21702-5012 | 10. SPONSORING / MONITORING AGENCY REPORT NUMBER |
|---|--|

|  |                     |
|--|---------------------|
| 11. SUPPLEMENTARY NOTES<br>Report contains color | <b>20030122 075</b> |
|--|---------------------|

|   |                        |
|---|------------------------|
| 12a. DISTRIBUTION / AVAILABILITY STATEMENT<br>Approved for Public Release; Distribution Unlimited | 12b. DISTRIBUTION CODE |
|---|------------------------|

**13. ABSTRACT (Maximum 200 Words)**

The goal of this proposed project is to develop an automated technique to assist radiologists in estimating mammographic breast density.

During this project year, we have collected the database of cases that have corresponding magnetic resonance (MR) images and mammograms acquired in a previous project. We have developed methods and a graphical user interface to analyze MR breast images. The fibroglandular tissue in the MR breast images was segmented with a semi-automatic method. We are also developing methods and computer programs, referred to as Mammographic Density ESTimator (MDEST), to automatically segment digitized mammograms and estimate the percent dense area on CC and MLO views. The preliminary results for analyzing 37 cases indicate strong correlation between mammographic density and the volumetric fibroglandular tissue estimated from MR breast images.

These results, although still preliminary, indicate that the usefulness of mammographic density as a surrogate for breast density estimation. The automated analysis will provide a reproducible and efficient method for analysis of mammographic density. When fully developed, MDEST is expected to contribute to the understanding of the relationship of mammographic density to breast cancer risk, detection, and prognosis, and to the prevention and treatment of breast cancer.

|  |                           |
|--|---------------------------|
| 14. SUBJECT TERMS<br>breast cancer, mammography, breast density, computer-assisted analysis, automated segmentation, risk monitoring | 15. NUMBER OF PAGES<br>32 |
|  | 16. PRICE CODE            |

|   |  |   |   |
|---|--|---|---|
| 17. SECURITY CLASSIFICATION OF REPORT<br>Unclassified | 18. SECURITY CLASSIFICATION OF THIS PAGE<br>Unclassified | 19. SECURITY CLASSIFICATION OF ABSTRACT<br>Unclassified | 20. LIMITATION OF ABSTRACT<br>Unlimited |
|---|--|---|---|

**(3) Table of Contents**

(1) Front Cover ..... 1

(2) Standard Form (SF) 298, REPORT DOCUMENTATION PAGE ..... 2

(3) Table of Contents ..... 3

(4) Introduction ..... 4

(5) Body ..... 5

    (A) Collection of Database

    (B) Development of Graphical User Interface (GUI) for Analysis of MR Images

    (C) Estimation of Percent Dense Area on Mammograms

    (D) Correlation between Percent Dense Area and Percent Volumetric Fibroglandular Tissue

(6) Key Research Accomplishments ..... 10

(7) Reportable Outcomes ..... 11

(8) Conclusions ..... 11

(9) References ..... 12

(10) Appendix ..... 12

#### **(4) Introduction**

Previous studies have found that there is a strong correlation between mammographic breast density and the risk of breast cancer. Mammographic breast density has been used by researchers in many studies to estimate breast cancer risk of epidemiological factors, monitor the effects of preventive treatments such as tamoxifen or dietary interventions, monitor the breast cancer risk of hormone replacement therapy, and investigate factors affecting mammographic sensitivity and cancer prognosis. However, most studies used Breast Imaging Reporting and Data System (BI-RADS) density rating as a measure of mammographic breast density, which contributes large inter- and intraobserver variations and may reduce the sensitivity of the analysis.

The goal of this proposed project is to develop a fully automated technique to assist radiologists in estimating mammographic breast density. We hypothesize that the computerized technique can accurately and efficiently segment the dense area on digitized or digital mammograms, thereby eliminating inter- and intra-observer variations. The dense area as a percentage of total breast area thus estimated will be more consistent and reproducible than radiologists' subjective BI-RADS rating. To accomplish this goal, we will (1) collect a large database of normal mammograms, including digitized film mammograms and digital mammograms, for training and testing the dense area segmentation program; (2) evaluate the correlation between the radiologists' breast density classification based on BI-RADS lexicon and the percent breast dense area; and (3) study the correlation of percent breast dense area between different views of the same breast and between the same view of the two breasts; and (4) investigate the correlation between the percent breast dense area estimated from mammograms and the volumetric dense breast tissue estimated from a data set of magnetic resonance (MR) breast images. These comparisons will provide important information regarding the consistency of the BI-RADS rating with the measured percent breast dense area, the appropriate measure of % dense area from different mammographic views, and the usefulness of using the percent breast dense area on mammograms as an indicator of volumetric breast tissue density.

It is expected that this project will produce a fully automated and effective tool for analysis of mammographic breast density, which can be applied to routinely acquired mammograms without special calibrations. This will facilitate studies of various factors associated with breast cancer risk and mammographic sensitivity, and monitoring the effects of interventional or preventive strategies. The image analysis tool will therefore contribute to the understanding of the relationship of density to breast cancer risk, detection, prognosis, and to the prevention and treatment of breast cancer.

## **(5) Body**

In the current project year (7/1/01-6/30/02), we have performed the following studies:

### **(A) Collection of Database**

We have obtained the research log (with IRB approval) of the previous research project that developed a dynamic MR imaging technique for the characterization of breast lesions. Based on the record, we found the mammographic files of 69 patients who have corresponding MR breast images and mammograms that are useful for the current study. The other cases have incomplete records, such as mammograms missing from the patient files, certain MR sequences not available. We will continue to track these cases to see if some of the missing information can be located. We have developed a database to categorize the cases for our project. The database includes the digitized mammograms, the corresponding MR images, and the pathological information obtained from biopsy. We have digitized the mammograms and archived them in our jukebox. For the MR study, we have retrieved the digital files from the archive in the MR laboratory, transferred all the files to our jukebox, and extracted the pre-contrast sequences for our analysis.

The MR image series used in this study included coronal 3D T<sub>1</sub>-weighted pre-contrast images acquired with the following technique: coronal sections 2-5 mm thick, 32 slices; 3D Spoiled Gradient-Recalled Echo (SPGR); TE=3.3ms; TR=10ms, Flip=40°, matrix=256x128, FOV=28-32cm right/left, 14-16cm superior/inferior, scan time=2 min 38 sec. This 3D SPGR sequence produced full volume coverage of both breasts with contiguous image slices. An example of images from one breast is shown in Fig. 1. Although this is not the optimal pulse sequence for separating water and fat, the fibroglandular parenchyma (~water) and fatty tissue are well separated with the heavily T<sub>1</sub>-weighted acquisition and therefore the series was chosen for the study.

### **(B) Development of Graphical User Interface (GUI) for Analysis of MR Images**

We have developed a GUI for analysis of the MR images semi-automatically. The GUI was written based on Matlab in an AlphaStation. The GUI first displays all slices of the pre-contrast MR sequence of one breast and the corresponding mammogram of the same breast (Fig. 1). The user can switch between the craniocaudal (CC) or the mediolateral oblique (MLO) view mammogram for comparison. The computer then displays each MR slice sequentially (Fig. 2). For each slice breast boundary is first detected automatically. A low pass filtering is employed within the breast boundary to estimate the low-frequency gray level background trend due to the field non-uniformity of the breast coil. The low frequency background is subtracted from the original image. After background correction, the histogram within the breast region is determined and interactive thresholding is used to separate the fibroglandular tissue region (displayed as dark) from the fatty tissue (white) region. After the segmentation is performed for all slices, the total fibroglandular tissue volume in the breast is estimated by summing the dark voxels over all slices, and the total breast volume is estimated by summing all the voxels within the breast. The percent fibroglandular tissue volume can then be derived as the ratio of the total fibroglandular tissue volume to the total breast volume. Some of the segmentation steps are detailed below:

#### Breast segmentation

We performed the analysis for each individual breast. The breast region in the MR slices of the anterior portion of the breast can be easily segmented from the background by automatic edge detection. As the slices get close to the chest wall, the breast tissue merges with the chest tissue. Often there is no distinguishable boundary between the breast tissue and the chest tissue in these slices. An expert breast radiologist will inspect the computer segmentation on the GUI slice by slice and correct the edge location if necessary (Fig. 3). In our GUI, several options for boundary correction are available. The first option is to use a snake algorithm to push the initial boundary to be closer to the actual boundary. The user can determine when to stop the iteration. The second option is to use an active contour algorithm to push the initial boundary to the actual boundary. This is similar to the snake algorithm except that the energy terms are different. The third option is to manually move the edge, which is represented by a polygon with an edge point at each apex, to the user chosen location. The last option is to manually draw a new edge by choosing the apex points of a polygon.

### Background correction

Background correction is applied to the breast region within the detected boundary. We have evaluated two background correction methods: (1) A low pass filtering method in which the low frequency gray level background of the breast is estimated by low-pass filtering and subtracted from the original image. (2) A distance-weighted background estimation method in which a given pixel in the background image is calculated as the weighted sum of the four boundary pixels. The weights are estimated by the inverse distance from the breast boundary to the given pixel. The background image is then subtracted from the original image.

After comparison with a large number of images, it was found that the second method is more robust than the first. The first method tends to overestimate the background for images containing a large area of fibroglandular tissue. The second method can closely approximate the background gray level trend and correct for the non-uniform background in the original image.

### Gray level thresholding

Gray level thresholding is used to separate the fibroglandular tissue from the fatty tissue. We employ an interactive thresholding method in which the gray level histogram of the breast region is displayed on the GUI. The thresholded image where the dense tissue is displayed as dark voxels and fatty tissue is displayed in white is also displayed and updated instantly whenever the threshold is changed. By comparing the thresholded image and the original image side-by-side, the user can adjust the threshold, using the threshold slider under the histogram, until the fibroglandular tissue is extracted from the fatty background.

### Density mask

In many MR slices, the skin forms a ring of dark voxels around the breast boundary. To exclude these skin voxels from being counted as fibroglandular tissue, a density mask is defined by applying morphological erosion to the breast boundary to obtain a mask slightly smaller than the breast region. The user can choose the structure element size for the morphological

operation. The resulting density mask is displayed superimposed on the thresholded breast image so that the user can judge if the skin voxels are excluded from the mask region.

### Percent fibroglandular tissue volume calculation

After the segmentation process is applied to all slices of the MR sequence of the breast, all voxels within the density mask in each slice are summed over the entire breast to obtain the fibroglandular tissue volume in the breast. Similarly, the voxels within the breast boundary in each slice are summed over all slices to obtain the total volume of the breast. The ratio of the fibroglandular tissue volume to the total breast volume yields the percent volumetric fibroglandular tissue in the breast.

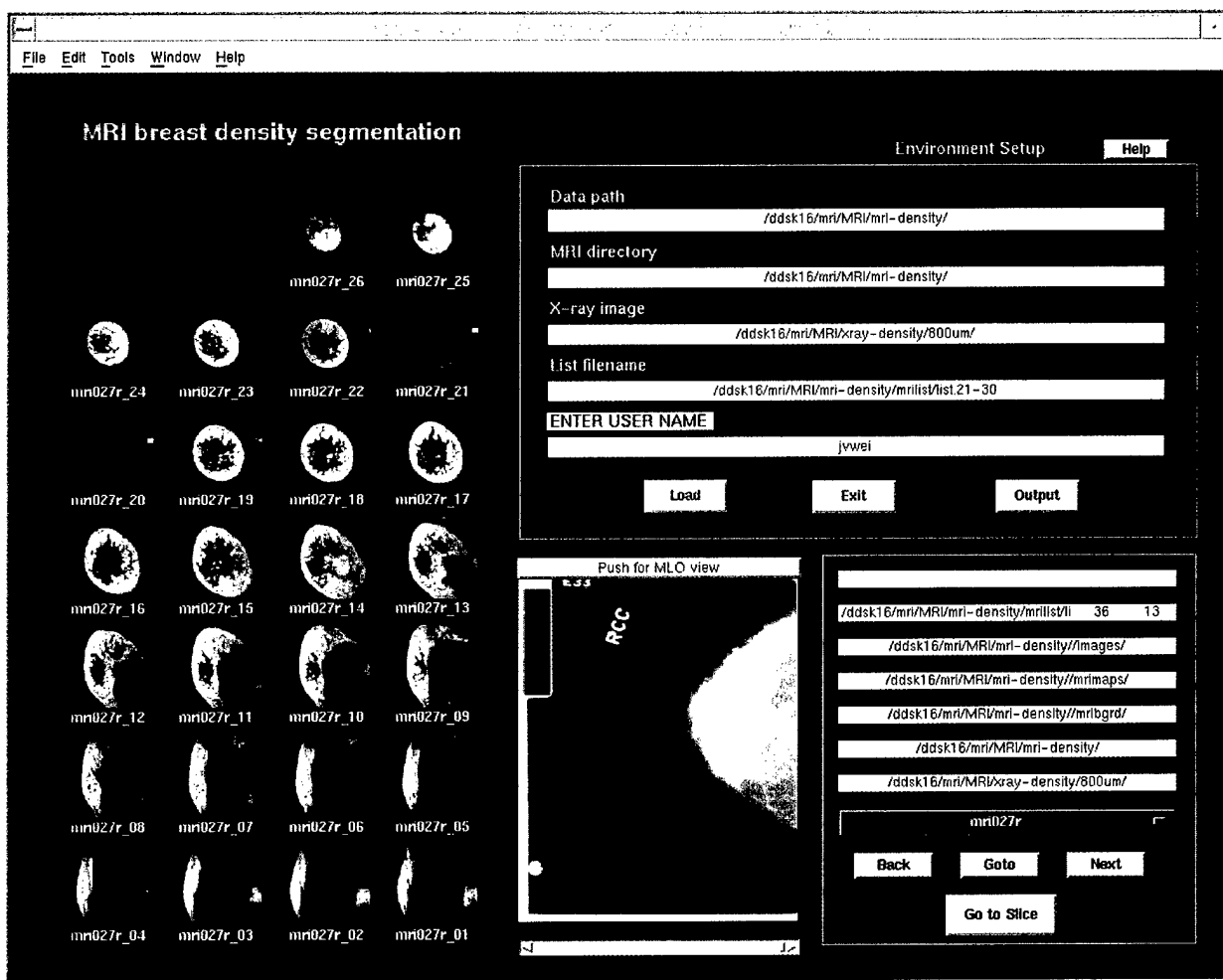


Fig. 1. The first screen of the graphical user interface that we developed for analysis of the MR breast images. The analysis was performed one breast at a time. The displayed slices on the left showed the MR sequence from the nipple to the chest wall of a coronal MR image sequence. The corresponding mammogram of the same breast is shown in the lower middle. The mammogram can be switched between the CC view and the MLO view.

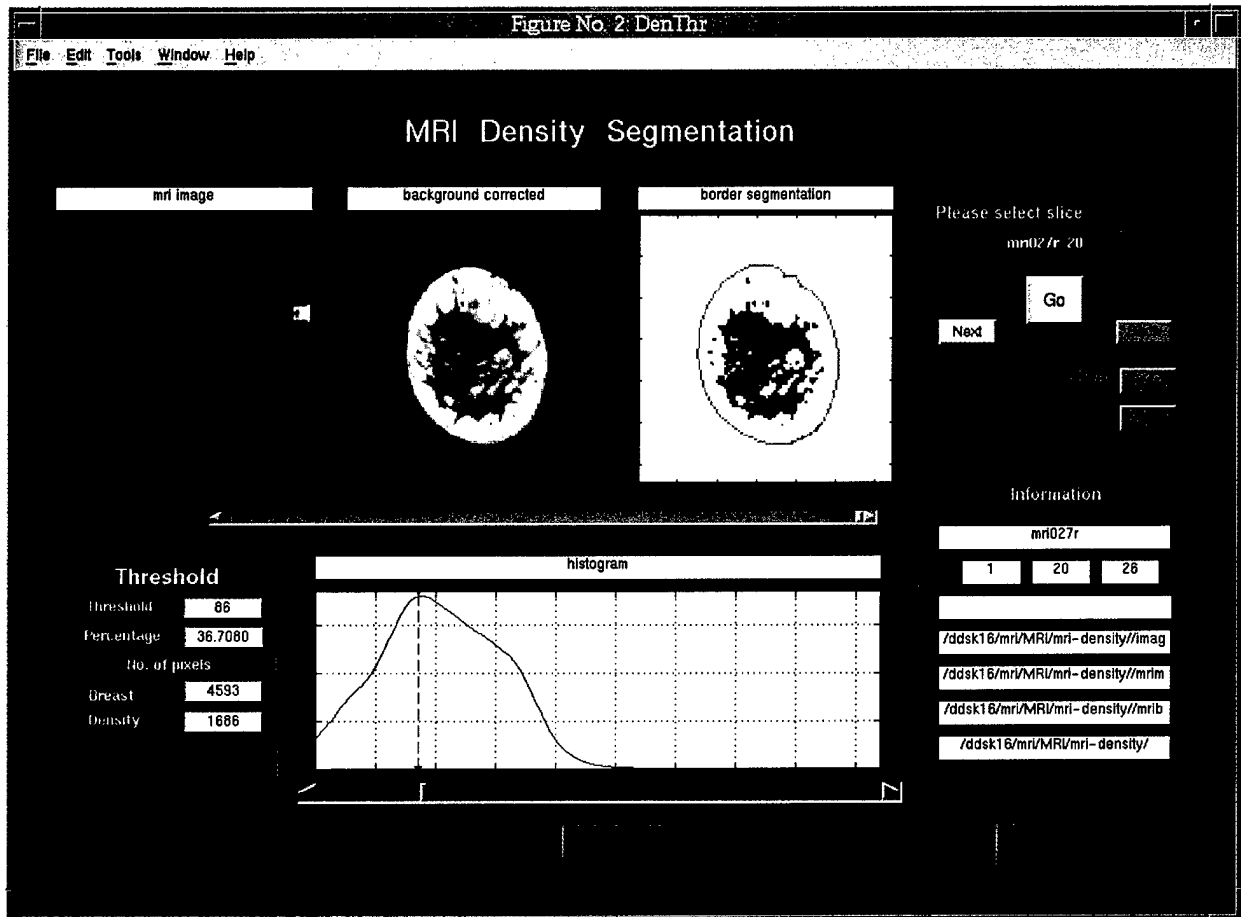


Fig. 2. The second screen of the GUI. The MR sequence is analyzed one slice at a time. The breast boundary was detected. The non-uniform gray level background was estimated by low-pass filtering and subtracted from the original image. The background corrected image is shown in the middle. The histogram of this image is obtained and displayed at the bottom of the screen. The user interactively thresholds the image. The image results from thresholding is shown on the right. The user subjectively determines the proper threshold for separately the fibroglandular tissue from the fatty tissue.

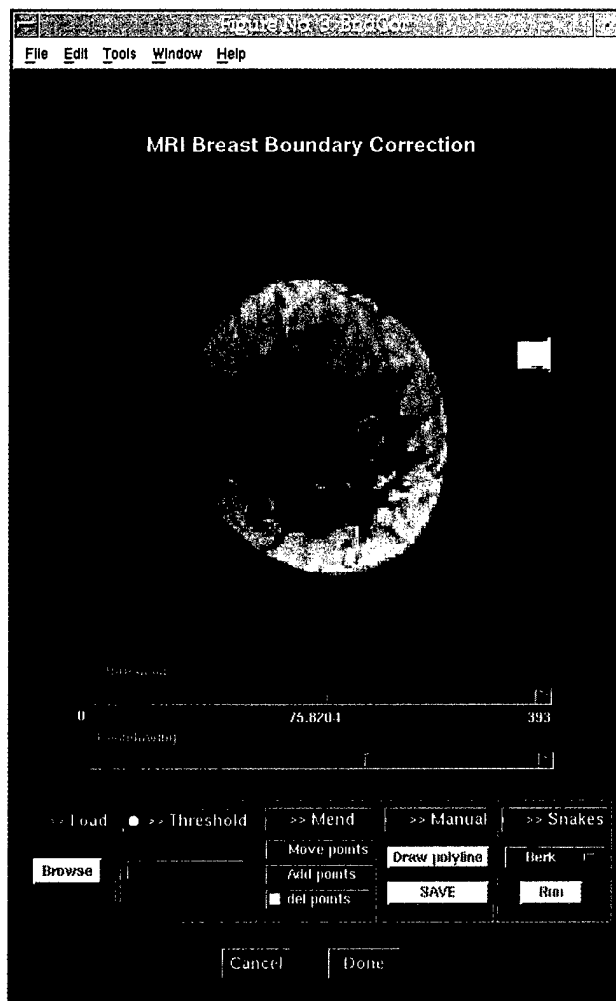


Fig. 3. The third screen of the GUI. If the user is not satisfied with the breast boundary displayed on the second screen, the user can click a boundary correction button on the second screen and get to this third screen. In this screen, the automatically detected edge is displayed on the breast slice. The user can use a snake algorithm to move the edge automatically, or manually adjust the edge location by moving the edge points individually.

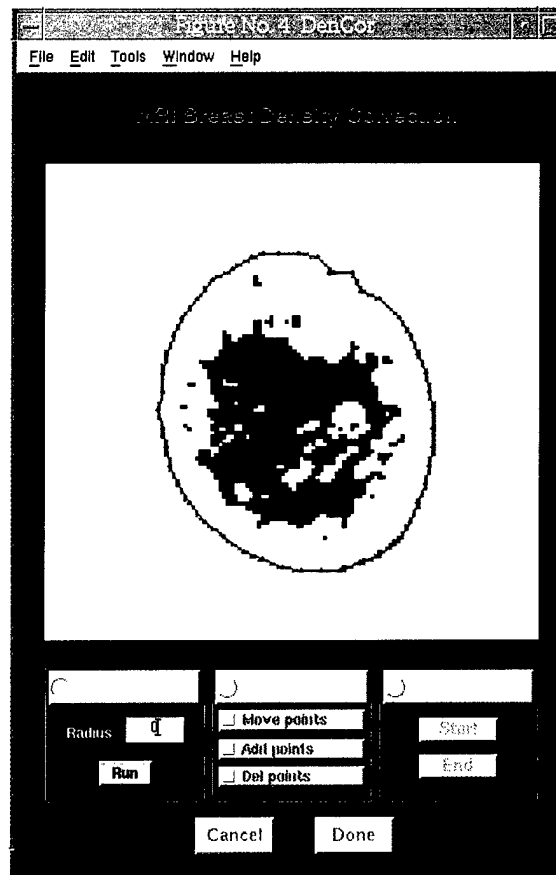


Fig. 4. The fourth screen of the GUI. After edge detection, background correction, and thresholding, the user can generate a “density mask” to define the region where the thresholded black voxels representing the fibroglandular tissue should be summed. The mask excludes the skin layer from the black voxels by applying morphological erosion to the breast boundary.

### (C) Estimation of Percent Dense Area on Mammograms

We are developing an automated image analysis tool, Mammographic Density ESTimator (MDEST), to assist radiologists in estimating mammographic breast density. MDEST performs dynamic range compression, breast boundary tracking, pectoral muscle segmentation for the MLO view, automatic thresholding based on gray level histogram analysis,

and calculates the percent dense area on a mammogram. In a preliminary study, we found that the correlation between the computer-estimated percent dense area and radiologists' manual segmentation was 0.94 and 0.91, respectively, for CC and MLO views, with a mean bias of less than 2%. As a result of this study, a journal article was published in the Medical Physics Journal [ref. 1].

**(D) Correlation between Percent Dense Area and Percent Volumetric Fibroglandular Tissue**

To date, we have performed segmentation of the MR images and their corresponding mammograms for 37 cases [ref. 2]. Scatter plots of the percent volumetric fibroglandular tissue versus the percent dense area on mammograms are shown in Fig. 5(a) and 5(b) for the CC- and MLO-view mammograms, respectively. The correlation of percent dense area of the CC and MLO views with the percent volumetric fibroglandular tissue on MR images was found to be 0.93 and 0.91, respectively, with a mean bias of 4.4%.

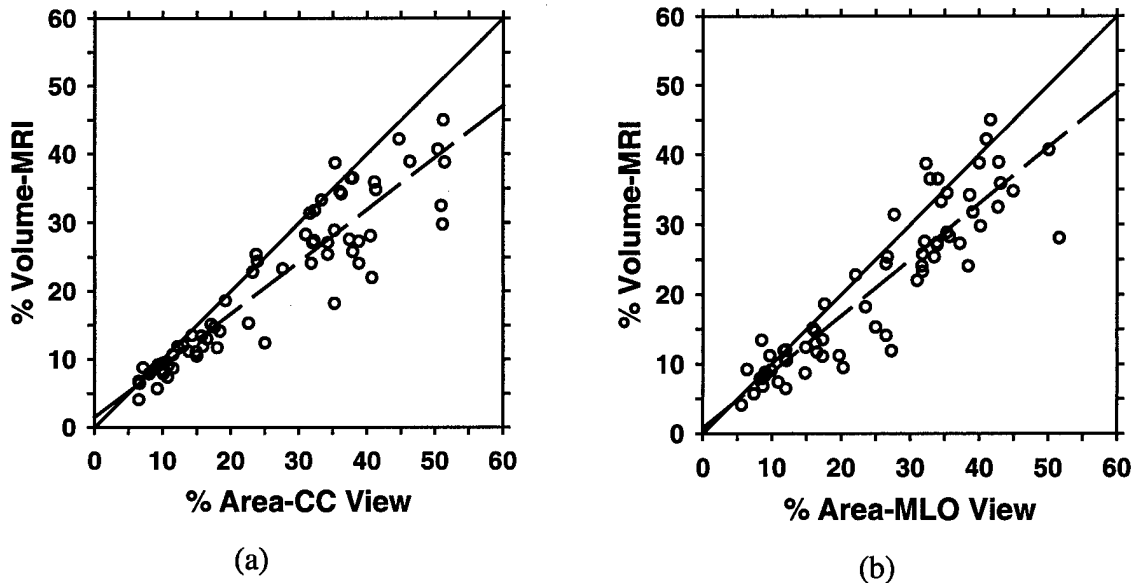


Fig. 5. Correlation of % volumetric fibroglandular tissue on MR images with % dense area on mammograms for 37 patients. The left and right breasts are plotted as separate data points on each graph. The dash lines are linear least squares fits to the data points.

**(6) Key Research Accomplishments**

- Collect the database of MR breast image sequence and the corresponding mammograms from the previous MR dynamic imaging study (Task 1 and Task 3)
- Develop the Graphical User Interface (GUI) for interactive segmentation of the MR images (Task 3).
- Develop preliminary methods for automated estimation of mammographic density (Task 2).

- Analyze 37 cases of the MR images and mammograms and study the correlation between the percent volumetric fibroglandular tissue and percent mammographic dense area (Task 3).
- Present preliminary results at the International Workshop for Digital Mammography (IWDM) in Bremen, Germany.

## **(7) Reportable Outcomes**

As a result of the support by the USAMRMC BCRP grant, we have conducted studies to investigate the correlation between mammographic density and MR volumetric fibroglandular tissue. The preliminary results were presented in an international conference. A conference proceeding paper will be published by the IWDM. In addition, we have developed a preliminary method for automated estimation of mammographic density, and performed a study to evaluate the correlation between the computer-determined mammographic density and radiologists' manual segmentation using interactive thresholding. The results were published in an article in the Medical Physics Journal.

### Journal Articles:

Zhou C, Chan HP, Petrick N, Helvie MA, Goodsitt MM, Sahiner B, Hadjiiski LM. Computerized image analysis: Estimation of breast density on mammograms. Medical Physics 2001; 28: 1056-1069.

### Conference Proceeding:

Chan HP, Hadjiiski LM, Roubidoux MA, Helvie MA, Paquerault S, Sahiner B, Chenevert T, Goodsitt MM. Breast density estimation: correlation of mammographic density and MR volumetric density. Proceedings of the 6th International Workshop on Digital Mammography. IWDM-2002. Bremen, Germany. June 22-25, 2002. (in press).

### Conference Presentation:

Chan HP, Hadjiiski LM, Roubidoux MA, Helvie MA, Paquerault S, Sahiner B, Chenevert T, Goodsitt MM. Breast density estimation: correlation of mammographic density and MR volumetric density. Poster presentation at the 6th International Workshop on Digital Mammography. IWDM-2002. Bremen, Germany. June 22-25, 2002.

## **(8) Conclusions**

During this project year, we have collected the database of cases that have corresponding magnetic resonance (MR) images and mammograms acquired in a previous project. We have developed methods and a graphical user interface to analyze MR breast images. The fibroglandular tissue in the MR breast images was segmented with a semi-automatic method.

We are also developing methods and computer programs, referred to as Mammographic Density ESTimator (MDEST), to automatically segment digitized mammograms and estimate the percent dense area on CC and MLO views. The preliminary results for analyzing 37 cases indicate strong correlation between mammographic density and the volumetric fibroglandular tissue estimated from MR breast images.

These results, although still preliminary, indicate that the usefulness of mammographic density as a surrogate for breast density estimation. The automated analysis will provide a reproducible and efficient method for analysis of mammographic density. When fully developed, MDEST is expected to contribute to the understanding of the relationship of mammographic density to breast cancer risk, detection, and prognosis, and to the prevention and treatment of breast cancer.

## **(9) References**

1. Zhou C, Chan HP, Petrick N, Helvie MA, Goodsitt MM, Sahiner B, Hadjiiski LM. Computerized image analysis: Estimation of breast density on mammograms. Medical Physics 2001; 28: 1056-1069.
2. Chan HP, Hadjiiski LM, Roubidoux MA, Helvie MA, Paquerault S, Sahiner B, Chenevert T, Goodsitt MM. Breast density estimation: correlation of mammographic density and MR volumetric density. Proceedings of the 6th International Workshop on Digital Mammography. IWDM-2002. Bremen, Germany. June 22-25, 2002. (in press).

## **(10) Appendix**

**Copies of the following publications are enclosed with this report:**

### Journal Article:

Zhou C, Chan HP, Petrick N, Helvie MA, Goodsitt MM, Sahiner B, Hadjiiski LM. Computerized image analysis: Estimation of breast density on mammograms. Medical Physics 2001; 28: 1056-1069.

### Conference Proceeding:

Chan HP, Hadjiiski LM, Roubidoux MA, Helvie MA, Paquerault S, Sahiner B, Chenevert T, Goodsitt MM. Breast density estimation: correlation of mammographic density and MR volumetric density. Proceedings of the 6th International Workshop on Digital Mammography. IWDM-2002. Bremen, Germany. June 22-25, 2002. (in press).

### Conference Poster Presentation:

Chan HP, Hadjiiski LM, Roubidoux MA, Helvie MA, Paquerault S, Sahiner B, Chenevert T, Goodsitt MM. Breast density estimation: correlation of mammographic density and MR

volumetric density. Poster presentation at the 6th International Workshop on Digital Mammography. IWDM-2002. Bremen, Germany. June 22-25, 2002.

# Computerized image analysis: Estimation of breast density on mammograms

Chuan Zhou, Heang-Ping Chan,<sup>a)</sup> Nicholas Petrick, Mark A. Helvie, Mitchell M. Goodsitt, Berkman Sahiner, and Lubomir M. Hadjiiski  
*Department of Radiology, The University of Michigan, Ann Arbor, Michigan 48109-0030*

(Received 15 September 2000; accepted for publication 4 April 2001)

An automated image analysis tool is being developed for the estimation of mammographic breast density. This tool may be useful for risk estimation or for monitoring breast density change in prevention or intervention programs. In this preliminary study, a data set of 4-view mammograms from 65 patients was used to evaluate our approach. Breast density analysis was performed on the digitized mammograms in three stages. First, the breast region was segmented from the surrounding background by an automated breast boundary-tracking algorithm. Second, an adaptive dynamic range compression technique was applied to the breast image to reduce the range of the gray level distribution in the low frequency background and to enhance the differences in the characteristic features of the gray level histogram for breasts of different densities. Third, rule-based classification was used to classify the breast images into four classes according to the characteristic features of their gray level histogram. For each image, a gray level threshold was automatically determined to segment the dense tissue from the breast region. The area of segmented dense tissue as a percentage of the breast area was then estimated. To evaluate the performance of the algorithm, the computer segmentation results were compared to manual segmentation with interactive thresholding by five radiologists. A "true" percent dense area for each mammogram was obtained by averaging the manually segmented areas of the radiologists. We found that the histograms of 6% (8 CC and 8 MLO views) of the breast regions were misclassified by the computer, resulting in poor segmentation of the dense region. For the images with correct classification, the correlation between the computer-estimated percent dense area and the "truth" was 0.94 and 0.91, respectively, for CC and MLO views, with a mean bias of less than 2%. The mean biases of the five radiologists' visual estimates for the same images ranged from 0.1% to 11%. The results demonstrate the feasibility of estimating mammographic breast density using computer vision techniques and its potential to improve the accuracy and reproducibility of breast density estimation in comparison with the subjective visual assessment by radiologists. © 2001 American Association of Physicists in Medicine. [DOI: 10.1118/1.1376640]

Key words: mammography, computer-aided diagnosis, breast density, breast cancer risk, image segmentation, thresholding

## I. INTRODUCTION

Breast cancer is one of the leading causes for cancer mortality among women.<sup>1</sup> One in every eight women will develop breast cancer at some point in their lives. The most successful method for the early detection of breast cancer is screening mammography. Currently, mammograms are analyzed visually by radiologists. Because of the subjective nature of visual analysis, qualitative responses may vary from radiologist to radiologist. Therefore, a computerized method for analyzing mammographic features would be useful as a supplement to the radiologist's assessment. Previous research efforts in computer-aided diagnosis (CAD) for breast cancer detection mainly concentrated on detection and characterization of masses and microcalcifications on mammograms by using computer vision techniques. It has been demonstrated that an effective CAD algorithm can improve the diagnostic accuracy of breast cancer characterization on mammograms, which, in turn, may reduce unnecessary biopsies. In this work, we are studying the feasibility of develop-

ing a CAD system for an analysis of breast density on mammograms. Studies have shown that there is a strong positive correlation between breast parenchymal density on mammograms and breast cancer risk.<sup>2-9</sup> The relative risk is estimated to be about 4 to 6 times higher for women whose mammograms have parenchymal densities over 60% of the breast area, as compared to women with less than 5% of parenchymal densities.

An important difference between breast density as a risk factor and most other risk factors is the fact that breast tissue density can be changed by dietary or hormonal interventions.<sup>6,10,11</sup> Although there is no direct evidence that changes in mammographic breast densities will lead to changes in breast cancer risk, the strong correlation between breast density and breast cancer risk has prompted researchers to use mammographic density as an indicator for monitoring the effects of intervention as well as for studying breast cancer etiology.<sup>6,11-13</sup>

Different methods have been used for the evaluation of

mammographic breast density. Earlier studies used a subjective visual assessment of the breast parenchyma primarily based on the four patterns described by Wolfe<sup>2</sup> (N1 is comprised entirely of fat; P1 has up to 25% nodular densities; P2 has over 25% nodular mammographic densities; DY contains extensive regions of homogeneous mammographic densities). The subjectivity in classifying the mammographic patterns introduced large variability in the risk estimation. Later studies used more quantitative estimates, such as planimetry, to measure the dense area in the breast manually outlined by radiologists on mammograms.<sup>3,7</sup> These studies indicate that the percentage (%) of mammographic densities relative to the breast area can predict the breast cancer risk more accurately than a qualitative assessment of mammographic patterns. Warner *et al.*<sup>15</sup> conducted a meta-analysis of the studies published between 1976 and 1990 to investigate the effect of different methods of classification on estimates of cancer risk. They found that the mammographic parenchymal pattern does correlate with the breast cancer risk. The magnitude of the risk varies according to the method used to evaluate the mammograms. With the quantitative estimates of mammographic density, the difference in risk between the highest and the lowest risk category is substantial and is greater than the risks associated with most other risk factors for breast cancer. More recent studies used fractal texture and the shape of the gray level histogram<sup>14</sup> to quantify the parenchymal pattern or used interactive thresholding on digitized mammograms to segment the dense area.<sup>11,15</sup> It was reported that the thresholding method provided a higher risk value than the texture measure or the histogram shape.<sup>16</sup> Other researchers have attempted to calculate a breast density index to model the radiologists' perception.<sup>17</sup>

In clinical practice, radiologists routinely estimate the breast density on mammograms by using the BI-RADS lexicon as recommended by the American College of Radiology<sup>18</sup> in order to provide a reference for mammographic sensitivity. Because of the lack of a quantitative method for breast density estimation, researchers often use the BI-RADS rating for monitoring responses to preventive or interventional treatment and the associated changes in breast cancer risk.<sup>19</sup> We have found that there is a large interobserver variability in the BI-RADS ratings among experienced mammographers.<sup>20,21</sup> An automated and quantitative estimation, as investigated in this study, will provide not only an efficient means to measure mammographic density, but also a reproducible estimate that will reduce the inter- and intraobserver variability of mammographic density measurements. This image analysis tool will therefore allow researchers to study more definitively the relationship of mammographic density to breast cancer risk, detection, prognosis, and mammographic sensitivity, and to better monitor the response of a patient to preventive or interventional treatment of breast cancers.

In this paper, we will describe the image processing techniques used in our automated breast density segmentation algorithm. The performance of the computer segmentation was evaluated by a comparison with the average segmenta-

tion by 5 radiologists using interactive thresholding in the same data set.

## II. MATERIALS AND METHODS

### A. Database

A data set consisting of 260 mammograms of 65 patients was used for the development of the histogram analysis method in this study. Each case contains the craniocaudal (CC) view and the mediolateral oblique (MLO) view of both breasts of the patient. The first 50 mammograms were consecutive screening cases from the patient files in the Radiology Department at the University of Michigan. After data analysis, it was found that there were very few dense breasts in the initial data set. An additional 15 cases visually judged by radiologists to be dense breasts were then randomly selected and mixed with the initial set. The images were processed individually without knowing their BI-RADS categories. The mammograms were acquired with mammography systems approved by the Mammography Quality Standards Act (MQSA) and were digitized with a LUMISYS 85 laser film scanner with a pixel size of  $50 \mu\text{m} \times 50 \mu\text{m}$  and 4096 gray levels. The gray levels are linearly proportional to optical densities (O.D.) from 0.1 to greater than 3 O.D. units. The nominal O.D. range of the scanner is 0–4 with large pixel values in the digitized mammograms corresponding to low O.D. The full resolution mammograms were first smoothed with a  $16 \times 16$  box filter and subsampled by a factor of 16, resulting in  $800 \mu\text{m} \times 800 \mu\text{m}$  images of approximately  $225 \times 300$  pixels in size for small films and  $300 \times 375$  pixels for large films.

### B. Breast segmentation and image enhancement

The breast image is first segmented from the surrounding image background by boundary detection. The detected boundary separated the breast from other background features such as the directly exposed area, patient identification information, and lead markers. The density analysis was performed only within the breast region. An automated breast boundary tracking technique developed previously<sup>22,23</sup> was modified to improve its performance. Briefly, the technique used a gradient-based method to search for the breast boundary. The background of the image was estimated initially by searching for the largest background peak from the gray level histogram of the image. After subtracting this background level from the breast region, a simple edge was found by a line-by-line gradient analysis from the top to the bottom of the image. The criterion used in detecting the edge points was the steepness of the gradient of four adjacent pixels along the horizontal direction. The steeper the gradient, the greater the likelihood that an edge existed at that corresponding image point. The simple edge served as a starting point for a more accurate tracking algorithm that followed. The tracking of the breast boundary started from approximately the middle of the breast image and moved upward and downward along the boundary. The direction to search for a new edge point was guided by the previous edge points. The edge

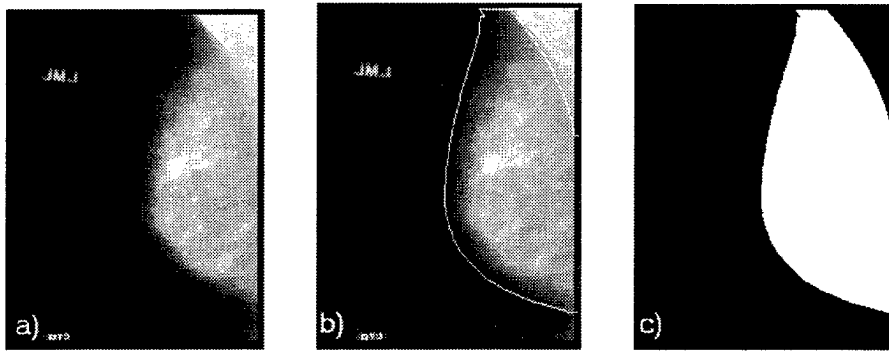


FIG. 1. (a) A mammogram from our image database; (b) the image superimposed with the detected breast boundary and pectoral muscle boundary; (c) the binary map of the segmented breast region.

location was again determined by searching for the maximum gradient along the gray level profile normal to the tracking direction. Since the boundary tracking was guided by the simple edge and the previously detected edge points, it could steer around the breast boundary and was less prone to diversion by noise and artifacts. The accuracy of the boundary tracking technique was evaluated in our previous study<sup>23</sup> by quantifying the root-mean-square differences between the detected and manually identified breast boundaries. In the current study, the performance of the boundary tracking technique for this data set was determined by superimposing the detected boundary on the breast image and visually judged if the detected boundary coincided with the perceived breast boundary. The breast image and its boundary were displayed by appropriately adjusting the contrast and brightness. Incomplete, jagged and mistracked boundaries were considered incorrect tracking.

The unexposed film area around the film edges was detected automatically. After the breast boundary was found, a region growing algorithm was used to fill the enclosed breast region. The result was a binary map that distinguished the breast region from the background areas. An example of the tracked breast boundary and the breast binary map is shown in Figs. 1(a)–1(c).

For the MLO view mammograms, an additional step has to be performed for segmentation of the pectoral muscle. The initial edge in the pectoral region was found as the maximum gradient point by a line-by-line gradient analysis from the chest wall to the breast boundary. The false pectoral muscle edge points were discarded by an edge validation process. First, a straight line was fitted to the initial edge points, and the points that did not lie close to the fitted line were removed. Second, the remaining edge points that were connected were identified by an 8-connectivity criterion. An edge segment was removed if its direction was inconsistent with the pectoral edge direction relative to the breast image. Finally, a second order curve was fitted to the remaining edge points to separate the pectoral muscle from the breast region. The pixels in the pectoral muscle region were excluded from the histogram analysis and breast area calculation. The accuracy of the pectoral muscle detection was also judged visually in this study, similar to the method used for the breast boundary described above. Figure 1 shows the pectoral muscle trimming result for an MLO view mammogram.

To facilitate histogram analysis, a dynamic range compression method was developed to reduce the gray level range of the histograms. With our digitization, the gray levels of the dense tissue are higher than those of the adipose tissue. Because of variations in exposure condition and breast thickness near the periphery, the gray level distribution corresponding to the breast parenchymal pattern is superimposed on a low frequency background that mainly represents the global variations in exposure. This low frequency background distorts the characteristic features of the histogram due to the density pattern. To reduce the distortion, an adaptive dynamic range compression technique was applied to the breast image. For a given breast image,  $F(x,y)$ , which contains low frequency background and higher frequency breast tissue structures, a smoothed image,  $F_B(x,y)$ , was obtained by applying a large-scale box filter to  $F(x,y)$  to remove the high frequency components while retaining the low frequency components. The image  $F_B(x,y)$  was then compressed by a scale factor  $k$ :

$$F_C(x,y) = kF_B(x,y). \quad (1)$$

To reconstruct the high frequency components,  $F_C(x,y)$ , was subtracted from a constant gray level  $G$ , and added to the original image,  $F(x,y)$ :

$$F_D(x,y) = G - F_C(x,y), \quad (2)$$

$$F_E(x,y) = F_D(x,y) + F(x,y). \quad (3)$$

Histogram analysis was applied to the dynamic-range-compressed image  $F_E(x,y)$ . Figure 2 shows an example of the resulting images and gray level histograms obtained from this procedure, where the size of box filter is  $35 \times 35$ , the scale factor  $k$  is 0.5, and the constant gray level  $G$  is the maximum gray level of the compressed image  $F_C(x,y)$ . The values of these parameters were chosen experimentally as a balance between reducing the dynamic range and preserving the image features in the compressed image.

### C. Breast density segmentation and estimation

A rule-based threshold technique was developed to segment the dense areas from the breast background. The histogram of the breast region on the dynamic-range-compressed mammogram was generated and smoothed. The histograms of these images in the database were analyzed to formulate an automatic thresholding routine. The histograms were

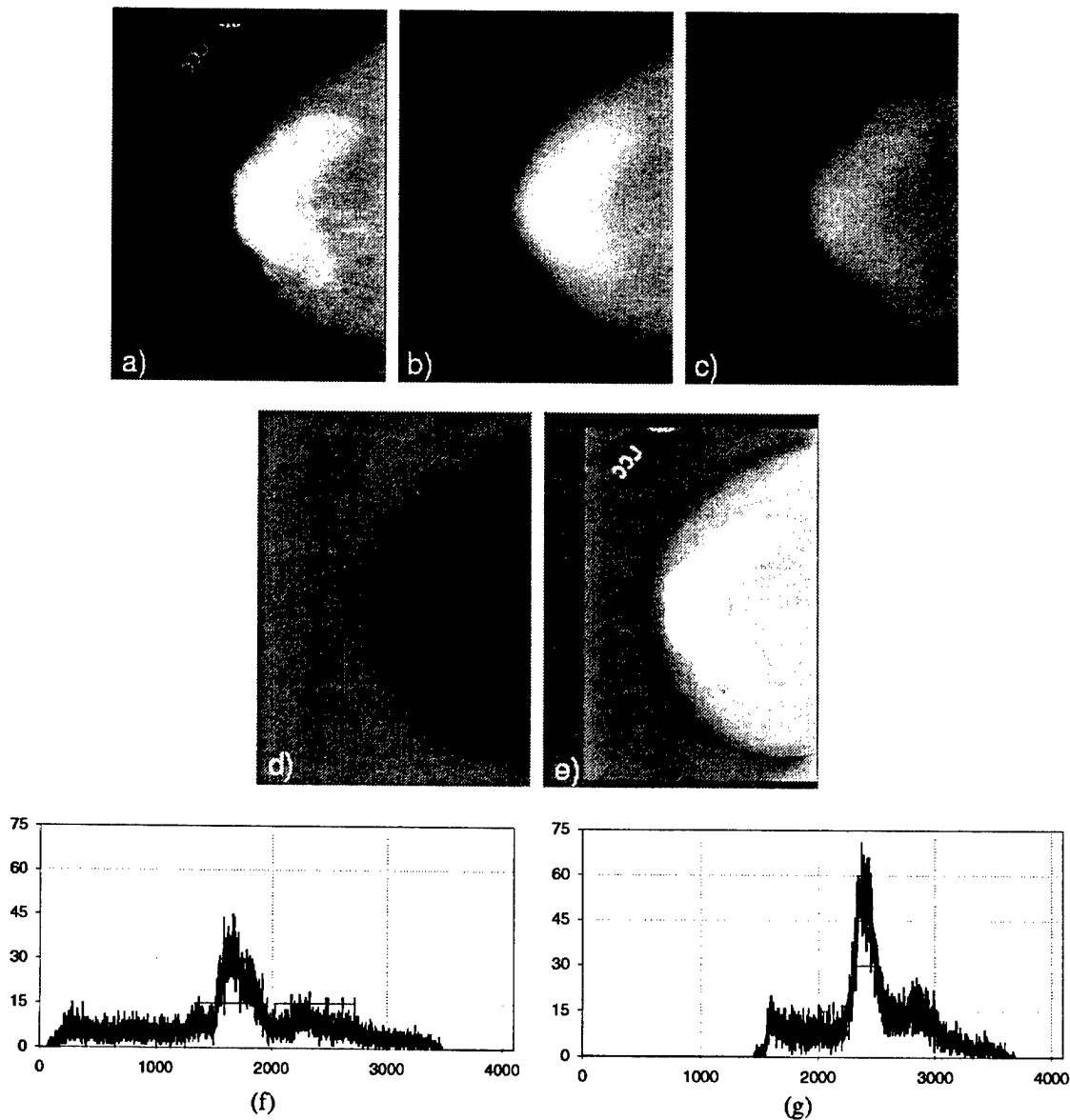


FIG. 2. (a) A typical mammogram from our image database; (b) the low frequency image  $F_B(x,y)$  obtained by an  $35 \times 35$  box filter; (c) the compressed image  $F_C(x,y)$ ; (d) the inverted image  $F_D(x,y)$ ; (e) the enhanced image  $F_E(x,y)$ ; (f) the gray level histogram within the breast region of the original image  $F(x,y)$ ; and (g) the gray level histogram of the breast region of the enhanced image  $F_E(x,y)$ .

grouped into four classes based on the characteristic shapes of their histograms. It was observed that the grouping corresponded approximately to the four BI-RADS breast density ratings: Class I corresponded to breasts of almost entirely fat, Class II corresponded to scattered fibroglandular densities, Class III corresponded to heterogeneously dense and Class IV corresponded to extremely dense breasts. Examples of typical histograms for these four classes are shown in Fig. 3. The histograms seemed to follow two basic patterns. In one pattern, there was only one dominant peak, which represented most of the breast structures in the breast region. In the other pattern, in addition to a large peak in the histogram, there was one or two smaller peaks on the right or left side of the large peak. In a majority of the cases, the smaller peak was distinguishable from the large one when the random fluctuation on the histogram was smoothed.

### 1. Peak detection and feature description

The gray level histogram within the breast area was generated and normalized, and passed through an averaging window to smooth out the random fluctuations. We estimated the window size to be in the range of 30 to 50 gray levels by experimentally evaluating the histogram shapes and density segmentation at different window sizes. Too small a window size cannot smooth out the fluctuation and too large a window size will blur the useful features. A window size of 30 was used in this study. The second derivative of every point on the histogram and its second derivative curve were computed. An example of the histogram and its second derivative curve are shown in Fig. 4. The zero crossing locations were detected by scanning for the positive-to-negative and negative-to-positive changes on the latter curve. If the second derivative was negative be-

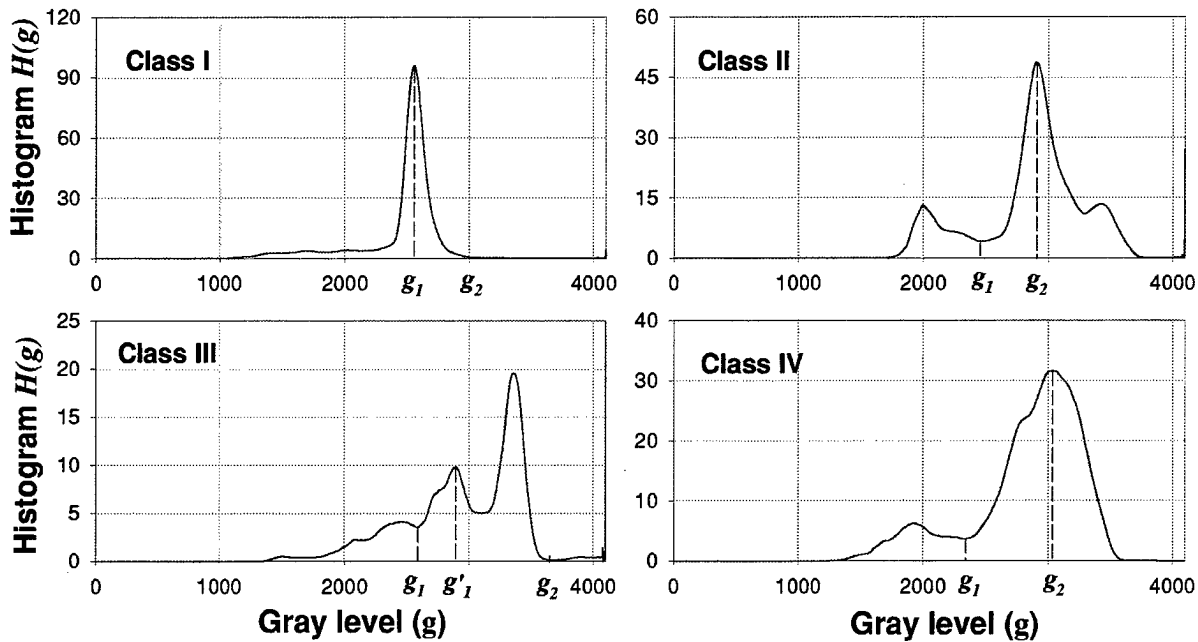


FIG. 3. Four typical classes of histograms and the setting of gray level interval  $[g_1, g_2]$  for the threshold calculation.

tween two zero crossing points, it indicated that a peak existed between these two points on the histogram. Normally, as shown in Fig. 4, a peak included the peak point  $P_0$  and two valley points  $P_1$  and  $P_2$  located on the two sides of the peak point. The peak point  $P_0$  was determined by searching for the maximum histogram value between the zero crossing points  $Z_2$  and  $Z_3$ , and the  $P_1$  and  $P_2$  points were obtained by searching for the point with minimum histogram value between zero crossing points  $Z_1, Z_2$  and  $Z_3, Z_4$ , respectively.

The following peak features can be defined by peak point  $P_0$  and valley points  $P_1$  and  $P_2$ :

$$\text{Energy: } E = \frac{1}{A} \sum_{i=P_1}^{P_2} f(i) * f(i), \quad (4)$$

$$\text{left-side energy: } E_L = \frac{1}{A} \sum_{i=P_1}^{P_0} f(i) * f(i), \quad (5)$$

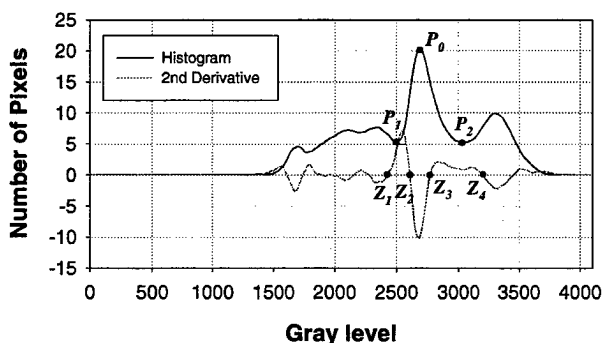


FIG. 4. The gray level histogram (solid curve) and the second derivative (dot) curve.  $P_0$  is the peak point,  $P_1$  and  $P_2$  are the valley points of the peak on the two sides of the peak point  $P_0$ . Points  $Z_1, Z_2, Z_3$  and  $Z_4$  are zero crossing points on the second derivative curve, which are used for searching the points  $P_0, P_1$  and  $P_2$ .

$$\text{right-side energy: } E_R = \frac{1}{A} \sum_{i=P_0}^{P_2} f(i) * f(i), \quad (6)$$

$$\text{likelihood: } L = E/E', \quad (7)$$

where  $f(\cdot)$  is the histogram,  $A$  is the total energy of the entire histogram and  $A = \sum_{i=0}^N f(i) * f(i)$ ,  $N$  is the maximum gray level of the histogram.  $E'$  is the energy calculated by approximating the histogram in the interval  $[P_1, P_2]$  using two straight lines,  $P_1P_0$  and  $P_0P_2$ . The energy  $E$  of the peak is used to compare the sizes of the peaks on the histogram, higher energy means bigger size of the peak.  $E_L$  and  $E_R$  split the energy  $E$  into two parts from the peak point for calculating the ratio of the energy in these two parts. The likelihood  $L$  describes how close the real peak is to the triangle represented by the three points  $P_0, P_1$  and  $P_2$ .

## 2. Rule-based histogram classification

A rule-based histogram classifier was developed to classify the gray level histogram of the breast area into four classes. As shown in Fig. 3, a typical Class I breast is almost entirely fat, it has a single narrow peak on the histogram. Class II has scattered fibroglandular densities, it has two peaks, other than the tail part on the left, on the histogram, with the smaller peak on the right of the bigger one. Class III is heterogeneously dense, it also has two peaks, but the smaller peak is on the left of the bigger one. Class IV is extremely dense, which has a single dominant peak on the histogram, but it is wider compared with the peak in the Class I histogram, and a second small peak sometimes occurs to the left of the main peak.

The classification is performed in two steps. In the first step, the computer determines whether there is only one single peak in the histogram. The biggest peak (main peak)

$P_M$  and its location are detected by comparing the energy of the peaks on the histogram. The single peak feature is mainly determined by the energy  $E$  under the main peak and the features  $E_L$  and  $E_R$ . If the histogram is found to have a single-peak pattern, in general, a narrow peak corresponds to very fatty breast (Class I), and a wider peak corresponds to very dense breast (Class IV). However, in some cases, the histogram of these two classes is very similar, as discussed below (Fig. 9), and it is difficult to distinguish them by their gray level histogram distributions. Two additional image features were analyzed to classify very fatty and very dense breasts. One feature is the gray level standard deviation (Std) in the entire breast area, defined as

$$\text{Std} = \left( \frac{1}{N} \sum_{x \in \text{MAP}} \sum_{y \in \text{MAP}} (f(x,y) - \bar{f}(x,y))^2 \right)^{1/2}, \quad (8)$$

where MAP is the breast binary map region,  $N$  is the pixel numbers within MAP. Another feature is the number of single pixels and single pixel-size holes (NSH) counted in the breast area of a segmented binary image using the biggest histogram peak point  $P_M$  as a threshold. For a very fatty mammogram, the breast mainly consists of a fatty background with some fibrous structures and fibroglandular tissue scattered in the breast area. The NSH value was found to be larger (greater than 50 pixels on average), and Std smaller (less than 500 on average), compared with a mammogram of a very dense breast.

In the second step, if the histogram is found to have more than one peak, decision rules are used to decide if the second major peak is on the left side or on the right side of  $P_M$  by the features  $E$ ,  $E_L$ ,  $E_R$  and  $L$ , and the relative position of the two peaks. If the second major peak is on the right, then the histogram is classified to be Class II; otherwise, it is classified to be Class III.

### 3. Gray level thresholding

Gray level thresholding is essentially a pixel classification problem. Its objective is to classify the pixels of a given image into two classes: one includes pixels with gray values that are below or equal to a certain threshold; the other includes those with gray values above the threshold. Thresholding is a popular tool for image segmentation, a variety of techniques have been proposed over the years. In our study, two threshold selection methods are used: one is the Discriminant Analysis (DA) method<sup>24</sup> and the other is the Maximum Entropy Principle (MEP) based method.<sup>25</sup> The DA method assumes that the image gray levels can be classified into two classes by a threshold. To estimate the threshold, a discriminant criterion based on the within-class variance and between-class variance is introduced. An optimal threshold is selected by the discriminant criterion to maximize the separability of the resultant classes in terms of gray levels. This method is well-suited for the cases where the gray level histogram is bimodal. In an ideal situation, the histogram has a deep and sharp valley between the two peaks representing objects and background, respectively, and the optimum corresponds to the gray level at the bottom of this valley. A

more detailed description of the DA method can be found in Appendix A.

For the MEP method, the optimal threshold value is determined by maximizing the *a posteriori* entropy subject to certain inequality constraints that are derived by means of special measures characterizing the uniformity and the shape of the regions in the image. As is well-known,<sup>26</sup> the maximum *a posteriori* probability can serve as a criterion to select *a priori* probability distributions when very little is known about the probability distribution. Compared with the DA method, MEP can provide a better thresholding result if the gray level histogram does not have a bimodal distribution. A more detailed description of the MEP method can be found in Appendix B.

The gray level histograms of the mammograms in our study are very complex, the histogram may be unimodal, bimodal or multi-modal. It is difficult to select an appropriate threshold by one general threshold selection method. Therefore, we combined both the DA and the MEP methods, to select a threshold according to the characteristic features of the histogram that has been classified into one of the four classes. Suppose  $f(g)$  is the gray level histogram of the breast area. Let  $T = \text{Method}(f(g)|g_1 < g < g_2)$  represent the threshold,  $T$ , that is selected by use of Method in the interval  $[g_1, g_2]$  of the histogram  $f(g)$ , where Method can be either the DA or MEP method. The settings of the interval  $[g_1, g_2]$  for the four classes are discussed below and shown in Fig. 3.

Class I: The histogram is unimodal so that the threshold is selected as

$$T = \text{MEP}(f(g)|g_1 < g < g_2),$$

where,  $g_1$  is the main peak point;  $g_2$  is the valley point on the right side of main peak.

Class II: The histogram is not unimodal and the histogram is classified as Class II; the threshold is selected by averaging two thresholds that are computed in two different intervals of the histogram by the DA method:

$$T_1 = \text{DA}(f(g)|g > g_1),$$

$$T_2 = \text{DA}(f(g)|g > g_2),$$

$$T = (T_1 + T_2)/2,$$

where  $g_1$  is the valley on the left of the main peak;  $g_2$  is the main peak point.

Class III: The histogram is not unimodal; there are two possibilities in the histogram distribution: there is a valley between the main peak and its left side peak, as shown in Fig. 3, or no obvious valley exists between the main peak and its left side peak. In two different intervals of the histogram, two thresholds are computed as

$$T_1 = \text{DA}(f(g)|g_1 < g < g_2),$$

$$T_2 = \text{DA}(f(g)|g'_1 < g < g_2),$$

where  $g_1$  is the left valley point of the left-side peak ( $P_{LM}$ ) of the main peak,  $g'_1$  is the peak point of  $P_{LM}$  and  $g_2$  is right valley point of the main peak. If there is an obvious valley,  $T = (T_1 + T_2)/2$ , otherwise  $T = T_1$ .

Class IV: Since the histogram is considered unimodal, the threshold is computed by the MEP method,  $T = \text{MEP}(f(g)|g_1 < g < g_2)$ , where,  $g_1$  is the left valley point of the main peak;  $g_2$  is the main peak point.

#### D. Radiologists' segmentation of dense breast tissue

In order to evaluate the accuracy of the computer segmentation method, the computer segmentation results were compared to radiologists' manual segmentation in the data set of 65 patient cases. Details of the observer study for estimation of the breast density and statistical analysis of the results were discussed elsewhere.<sup>27</sup> Briefly, a graphical interface was developed for displaying the mammograms and recording the observer's evaluation. The CC-view and MLO-view mammograms for a given breast were displayed side-by-side; a radiologist observer examined the mammograms and gave a BI-RADS rating and a visual estimation of the percent breast density with 10% increments. After the subjective evaluation, each view was displayed sequentially, together with the histogram of the dynamic-range-compressed image. The radiologist would interactively choose a threshold by moving a slider along the abscissas of the histogram plot. The segmented binary image, displayed side-by-side with the mammogram, would change instantaneously when the threshold was changed. The radiologist could inspect if the segmented area corresponded to the dense area on the mammogram. Once the radiologist was satisfied with the segmentation of the dense area, the gray level threshold and the percent dense area derived from this threshold were recorded. The display then moved to the next view of the same breast for evaluation. The mammograms of the other breast for the same patient would then be displayed and evaluated in the same way. The entire process was repeated for each patient until all patients in the data set were evaluated.

Five MQSA-approved radiologists participated in the experiment. To familiarize the radiologists with the procedures and to assist them in their visual estimation of the percent breast density, we had them trained on a separate set of 25 patient cases prior to the evaluation of the actual data set. During the training session, the computer displayed the percent breast dense area to the radiologist, which was obtained by the radiologist's interactive thresholding of the image. The radiologist could then compare the manually segmented percentage with their visually assessed percent density for the image. This feedback helped "calibrate" the radiologists' visual estimates of the percent dense breast area. The percent dense area obtained by interactive thresholding was not displayed during the actual study.

### III. RESULTS

An example of a typical mammogram from each of the four classes and its corresponding enhanced image, its histogram, the selected threshold and the segmented image are shown in Figs. 5(a)–5(d), respectively.

The average percent breast density obtained from manual segmentation by the five trained radiologists for each mammogram was used as the "true standard" of the percent

breast density for that mammogram. The breast region was segmented by the breast boundary tracking technique, and the pectoral muscle was trimmed for the MLO-view mammograms. The breast boundary was accurately tracked on 92.3% (240/260) of the mammograms, and the pectoral muscle was correctly trimmed on 74.6% (97/130) of the MLO views. The histograms of 6% (8 CC views and 8 MLO views) of the breast regions did not exhibit the typical characteristic features of the four classes and were misclassified by the computer, resulting in poor segmentation of the dense region.

Figure 6 shows a comparison of the percent breast density visually estimated by radiologists against the true standard for the 94% of the 260 mammograms that were classified correctly by the computer. Table I summarizes the comparison of the radiologists' visual estimates with the true standard. The "difference" between the estimated % breast density and the true standard was calculated for each case, and the mean and the standard deviation of this difference over all cases were estimated for each radiologist and shown in the table. Therefore, the mean difference was the average bias of the estimated % breast density from the true standard over all images in the data set. It can be seen that almost all radiologists had a positive bias, on average, when they visually estimated mammographic density, except for Radiologist 5 who had a small negative average bias on the CC-view reading. For a given radiologist, the over-estimation increased as the breast density increased. Although the correlation coefficients were high, ranging from 0.90 to 0.95, the deviations from the diagonal line were systematic. The average bias from the true standard varied from less than 1% to 11%, depending on the radiologist. The root-mean-square (RMS) errors of the five radiologists relative to the true standard ranged from 7.5% to 16.3%.

Figure 7 shows the comparison of the percent breast density between the computer segmentation and the true standard for the 94% of mammograms whose histograms were considered to be correctly classified. There was a trend of over-estimation in the very fatty breasts. In the medium dense range, the variances from the true standard were high. Some images had a large deviation from the diagonal line, indicating that the threshold was incorrectly determined. Table II summarizes the comparison between the computer performance and the true standard. For the CC views with correct histogram classification, the correlation between the computer-estimated percent dense area and the true percent breast density was 0.94, and between the computer and the radiologists' average visual estimate was 0.87 (not plotted). These correlation coefficients were 0.91 and 0.82, respectively, for the MLO views with correct classification. Although the correlation coefficients of the computer segmentation with the true standard were not better than those of the visual estimates, the average biases of the computer segmentation from the true standard were less than 2%, which were substantially less than those of visual estimates (Table I). This indicates that computerized segmentation is a good alternative to manual segmentation although variances of the automated method will need to be further reduced. The RMS

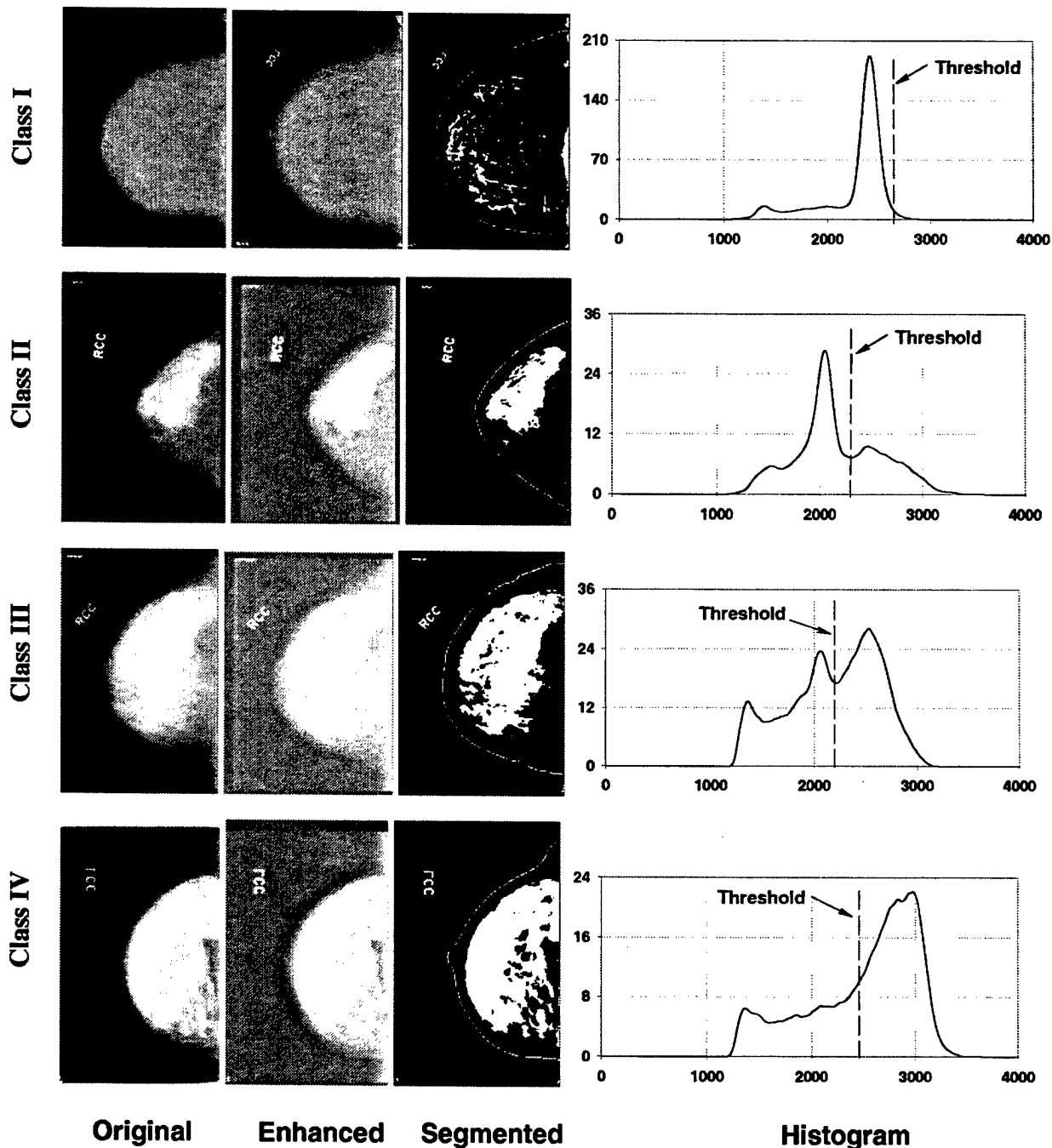


FIG. 5. Four classes of typical mammograms and corresponding enhanced and segmented image, histogram and threshold.

errors of the computer segmentation were also less than those of the radiologists' visual estimates, at 6.1% and 7.2%, respectively, for the CC view and MLO view, when the histograms were correctly classified. The biases and RMS errors for the different subsets of images are also shown in Table II. It can be seen that correct histogram classification was the most important factor in reducing the biases and the RMS errors. The contributions by breast boundary detection and pectoral muscle segmentation were minor, on average, for improving the estimation of the percent dense breast area.

Figure 8 shows the comparison of the individual radiologists' manual segmentation against the true standard. For CC views, the RMS difference in the percent breast density be-

tween an individual radiologist's manual segmentation and the true standard varied from 2.9% to 5.9% among the five radiologists. For MLO views, the RMS difference varied from 2.8% to 6.2%. The average biases of the five radiologists ranged from -2.8% to 2.2% for the CC views and from -3.1% to 3.0% for the MLO views. The maximum biases of the five radiologists varied from 4.4% to 22.6% for the CC views and from 5.2% to 23% for the MLO views.

The five radiologists provided BI-RADS density ratings for each breast. Although the BI-RADS ratings exhibited large inter-observer variations,<sup>20</sup> it is interesting to compare the computer's histogram classification with the BI-RADS ratings. Since there were 260 images, each with 5 radiolo-

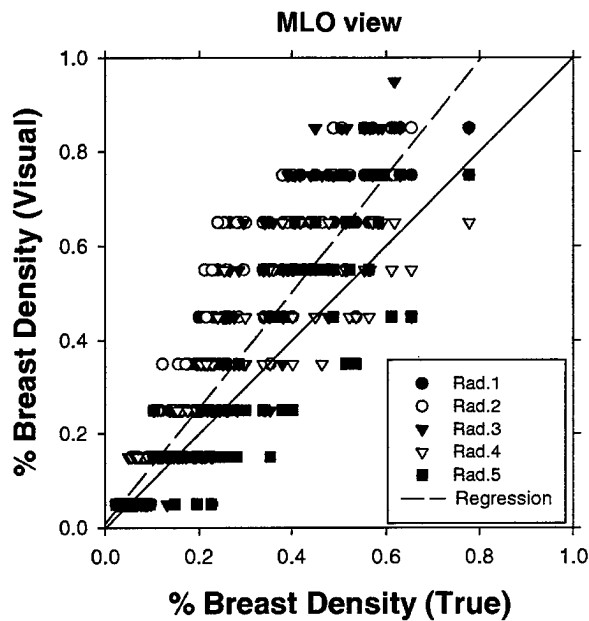


FIG. 6. A comparison of the percent breast density between five radiologists' visual estimates and the true standard. The dashed line represents the linear regression of all data points on the plot. The MLO view is shown. The trend for the CC view is similar.

gists' ratings, there were a total of 1300 rating comparisons. The comparison of the computer and the radiologists' BI-RADS ratings is shown in Table III. It was found that 87.4% of Class I classification have BI-RADS ratings 1 or 2, 92.0% of Class II classifications have density ratings 2 or 3, 83.4% of Class III classifications have density ratings 3 or 4

and 57.1% of Class IV classifications have density rating 4. More detailed analysis of the variability of radiologists' BI-RADS ratings was discussed by Martin *et al.*<sup>21</sup>

#### IV. DISCUSSION

Radiologists routinely estimate mammographic breast density using the four BI-RADS categories. In studies that require breast density estimation, radiologists' visual estimates of mammographic density were often used as the density measure. Our observer study indicates that interobserver variation between the BI-RADS ratings of five experienced radiologists ranged from  $-1$  to  $+1$ . The subjectively estimated percent dense area can deviate from the true standard by as much as 40%, as shown in Fig. 6. These results indicate the need to develop an objective method for the estimation of mammographic breast density in order to improve the accuracy and reproducibility of the estimation. A computerized image analysis method for mammographic breast density estimation will be a useful tool for study of breast cancer risk factors and for monitoring the change of breast cancer risk with preventive or interventional treatments.

In this study, we used the average of the percent breast area obtained with interactive thresholding by five experienced radiologists as the true standard. The gray level thresholding method used in this study could achieve a reasonable segmentation of the dense areas on the mammogram because the image was preprocessed with dynamic range compression. The image-based analysis of breast density will not provide the actual percentage of fibroglandular tissue in the breast volume. However, the previous studies that estab-

TABLE I. A comparison of the radiologists' visual estimate of mammographic breast density with the true standard. The "difference" was defined as the difference between the estimated % breast density and the true standard for each case, and the mean and the standard deviation of this difference are tabulated.

| Image subsets                  | No. of images | Radiologist | Correlation | RMS error | Mean difference | Std. dev. of difference |
|--------------------------------|---------------|-------------|-------------|-----------|-----------------|-------------------------|
| CC view:                       |               |             |             |           |                 |                         |
| All                            | 130           | Rad. 1      | 0.942       | 13.3%     | 6.9%            | 11.5%                   |
|                                |               | Rad. 2      | 0.931       | 14.5%     | 9.8%            | 10.7%                   |
|                                |               | Rad. 3      | 0.923       | 13.3%     | 6.3%            | 11.8%                   |
|                                |               | Rad. 4      | 0.934       | 7.5%      | 2.9%            | 7.0%                    |
|                                |               | Rad. 5      | 0.901       | 9.6%      | -1.4%           | 9.6%                    |
| Histogram correctly classified | 122           | Rad. 1      | 0.946       | 13.7%     | 7.2%            | 11.3%                   |
|                                |               | Rad. 2      | 0.936       | 14.7%     | 10.3%           | 10.8%                   |
|                                |               | Rad. 3      | 0.929       | 14.2%     | 6.7%            | 11.6%                   |
|                                |               | Rad. 4      | 0.929       | 7.7%      | 3.1%            | 7.1%                    |
|                                |               | Rad. 5      | 0.900       | 9.7%      | -1.3%           | 9.4%                    |
| MLO view:                      |               |             |             |           |                 |                         |
| All                            | 130           | Rad. 1      | 0.933       | 14.5%     | 8.3%            | 12.0%                   |
|                                |               | Rad. 2      | 0.914       | 16.1%     | 11.2%           | 11.5%                   |
|                                |               | Rad. 3      | 0.915       | 14.4%     | 7.7%            | 12.2%                   |
|                                |               | Rad. 4      | 0.919       | 8.8%      | 4.3%            | 7.7%                    |
|                                |               | Rad. 5      | 0.910       | 9.2%      | 0.1%            | 9.2%                    |
| Histogram correctly classified | 122           | Rad. 1      | 0.932       | 15.0%     | 8.3%            | 12.0%                   |
|                                |               | Rad. 2      | 0.914       | 16.3%     | 10.9%           | 11.4%                   |
|                                |               | Rad. 3      | 0.919       | 14.7%     | 7.8%            | 12.2%                   |
|                                |               | Rad. 4      | 0.916       | 9.0%      | 4.3%            | 7.7%                    |
|                                |               | Rad. 5      | 0.909       | 9.4%      | 0.3%            | 9.2%                    |

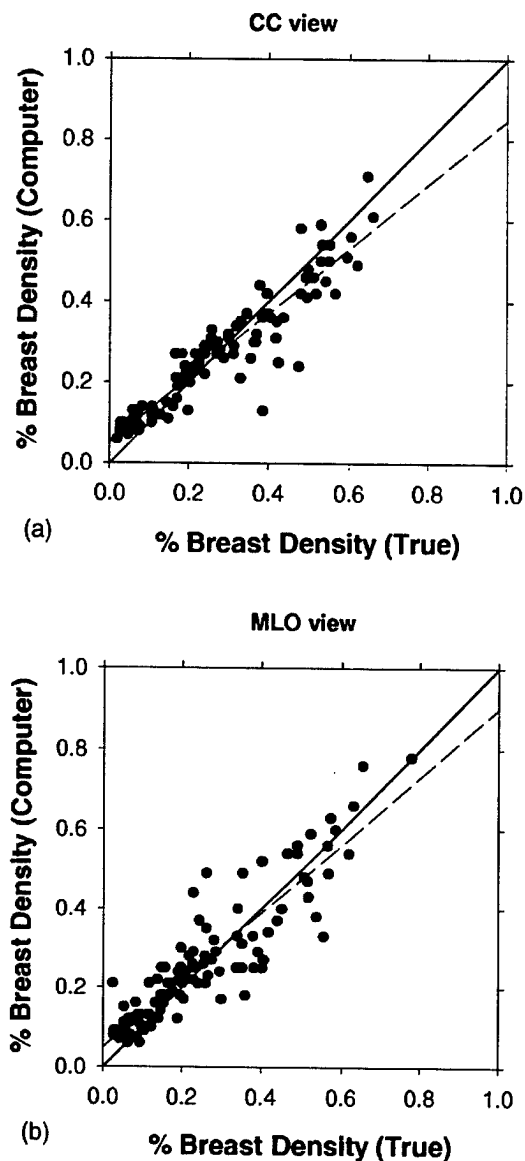


FIG. 7. A comparison of the percent breast density between the computer segmentation and the true standard. The dashed line represents the linear regression of the data on the plot. (a) CC view, (b) MLO view.

lished the correlation between breast density and breast cancer risk were all based on mammographic density. This indicated that mammographic density is a sufficiently sensitive marker for breast cancer risk, although it may be less accurate than volumetric density. An actual measurement of the percentage of fibroglandular tissue volume in the breast, for example, by x-ray penetration with correction for scatter and beam hardening, is difficult because it requires accurate x-ray sensitometry or phantom calibration for each image. These requirements will limit its use to a few laboratories that have specialized equipment and expert physicists. Magnetic resonance breast imaging can also provide volume measurement of dense tissue but it is expensive and not easily accessible. It can be expected that the estimation of mammographic breast density by a computerized image analysis method will be a more practical and viable approach, espe-

cially when direct digital mammography becomes more widely used in the future.

Our preliminary study indicates that breast density estimation can be performed automatically and accurately (Fig. 7). Although the accuracy of our current algorithm still needs to be improved, it can be seen that the computer segmentation can provide an estimate of the percent breast density with a very small bias (Table II). More importantly, computer segmentation will be more reproducible and consistent than visual estimates. This will improve the sensitivity of studies that depend on evaluation of the change in mammographic density over time or before and after a certain treatment.

In this study, we reduced the spatial resolution to a pixel size of  $800\ \mu\text{m} \times 800\ \mu\text{m}$  for image processing. The small matrix size of the reduced images improves the computational efficiency. The reduction in resolution has two major effects: reducing the image noise and blurring the details. Since the significant dense tissue in the breast that contributes to the parenchyma is relatively large compared to  $800\ \mu\text{m}$ , it is not expected that processing at this pixel size will have a strong effect on the accuracy of the estimated percent breast density. Differences in the segmented area may occur mainly along the boundary of the dense tissue region, but the effect may be averaged out statistically along boundaries of reasonable lengths. The residual errors in the estimation of the dense area should not be substantial in comparison with the inter- and intra-radiologists' variations in their manual segmentation.

Successful segmentation of dense tissue depends strongly on whether a mammogram can be classified correctly into a proper class. A successful classification will likely result in the selection of a near optimal threshold. Conversely, if a mammogram is classified into a wrong class, the threshold will be selected incorrectly. For the mammograms of very fatty breasts, the gray level histogram has the characteristics of Class I, which contains one large single peak. These histograms can be distinguished relatively easily from most of the other classes of histograms if those histograms exhibit the typical features. For mammograms of BI-RADS category 2 or 3, there are scattered fibroglandular or heterogeneous densities in the breast. A small peak may be located on the left or on the right, or on both sides of the main peak on the histogram. The histogram could be classified into Class I if the small peak is not large enough and is not detected as a second peak. Otherwise, it would be classified into Class II or Class III, depending on the location of that small peak relative to the main peak of the histogram. For the two-peak pattern histogram, the DA threshold selection method is robust if there is an obvious valley between the two peaks. If the valley is flat or not obvious, averaging the two thresholds obtained by the DA method in two different intervals, as designed for this study, can reduce the chance of calculating an incorrect threshold that differs greatly from the optimum, but it also reduces the chance of finding the optimal threshold. Overall, the rules designed for classification of the two-peak patterns seem to perform consistently well for this data set. One of the difficult situations is to distinguish between

TABLE II. A comparison of computer segmentation with the true standard. The "difference" was defined as the difference between the estimated % breast density and the true standard for each case, and the mean and the standard deviation of this difference are tabulated.

| Image subsets  | No. of images | Correlation | RMS error | Mean difference | Std. dev. of difference |
|--|---------------|-------------|-----------|-----------------|-------------------------|
| CC view:   |               |             |           |                 |                         |
| All  | 130           | 0.746       | 12.3%     | 1.3%            | 12.3%                   |
| Boundary correctly tracked                             | 120           | 0.780       | 11.4%     | 1.4%            | 11.4%                   |
| Histogram correctly classified                         | 122           | 0.943       | 6.1%      | 0.2%            | 6.2%                    |
| Boundary and histogram correctly done                  | 113           | 0.953       | 5.6%      | 0.8%            | 5.6%                    |
| MLO view:  |               |             |           |                 |                         |
| All  | 130           | 0.780       | 11.6%     | 1.9%            | 11.5%                   |
| Boundary correctly tracked                             | 120           | 0.766       | 11.9%     | 2.1%            | 11.7%                   |
| Histogram correctly classified                         | 122           | 0.914       | 7.2%      | 1.5%            | 7.1%                    |
| Pectoral muscle correctly trimmed                      | 97            | 0.733       | 11.6%     | 1.6%            | 11.6%                   |
| Boundary and histogram correctly done                  | 112           | 0.912       | 7.2%      | 1.7%            | 7.1%                    |
| Boundary, histogram and pectoral muscle correctly done | 83            | 0.891       | 7.1%      | 1.9%            | 6.8%                    |

Class I and Class IV, when the histogram of a very dense breast mimics that of a very fatty breast, as shown in Fig. 9. This image was correctly classified with the additional features, Std and NSH. However, there were other cases that failed in spite of the additional criteria. The large difference in the optimal threshold locations between these two classes will lead to a large error in the estimated percent breast density if the histogram is misclassified. Further study is needed to more accurately distinguish these two classes.

The dynamic range reduction technique reduces the variability of the gray level histograms and enhances their characteristics. This pre-processing facilitates the classification of the image into the correct class. There are many image smoothing techniques published in the literature. Low-pass filtering with a box filter is the simplest choice. The effec-

tiveness of background correction with a box filtered image depends on the box size. We found that a  $35 \times 35$ -pixel filter is a good balance between computation time and the capability to remove the high frequency components. The subtraction of the low-pass filtered image from the original image is a form of unsharp masking. The breast boundary is generally enhanced as shown in Fig. 2(e). The pixels at the enhanced breast boundary contribute a small peak to the left tail of the gray level histogram of the breast area. Moreover, if dense tissue is present close to the breast boundary, it may not be segmented correctly due to intensity reduction. Other low frequency estimation techniques such as wavelet decomposition will be investigated in future studies.

In this feasibility study, we used a small data set of mammograms to develop a rule-based classifier for the histogram analysis. Although a large fraction of the histograms manifest characteristic features that can be grouped into four classes, corresponding approximately to the four BI-RADS breast density ratings, there are many exceptions. One such example is shown in Fig. 9. This causes misclassification and incorrect thresholding by the histogram classifier. It will be

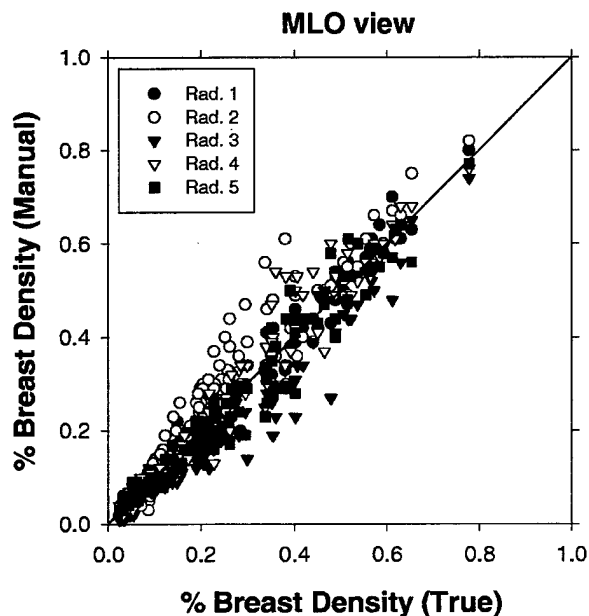


FIG. 8. A comparison of the percent breast density obtained from the five radiologists' manual segmentation with their average for the same mammograms. The MLO view is shown. The trend for the CC view is similar.

TABLE III. A comparison of computer classification and radiologists' BI-RADS breast density ratings.

| Computer classification | BI-RADS 1      | BI-RADS 2      | BI-RADS 3      | BI-RADS 4      | Total          |
|-------------------------|----------------|----------------|----------------|----------------|----------------|
| Class I                 | 210<br>(16.2%) | 262<br>(20.2%) | 52<br>(4%)     | 16<br>(1.2%)   | 540<br>(41.5%) |
| Class II                | 0<br>(0%)      | 92<br>(7.1%)   | 184<br>(14.2%) | 24<br>(1.8%)   | 300<br>(23.1%) |
| Class III               | 1<br>(0.1%)    | 52<br>(4%)     | 167<br>(12.8%) | 100<br>(7.7%)  | 320<br>(24.6%) |
| Class IV                | 5<br>(0.4%)    | 12<br>(0.9%)   | 43<br>(3.3%)   | 80<br>(6.2%)   | 140<br>(10.8%) |
| Total                   | 216<br>(16.6%) | 418<br>(32.2%) | 446<br>(34.3%) | 220<br>(16.9%) | 1300<br>(100%) |

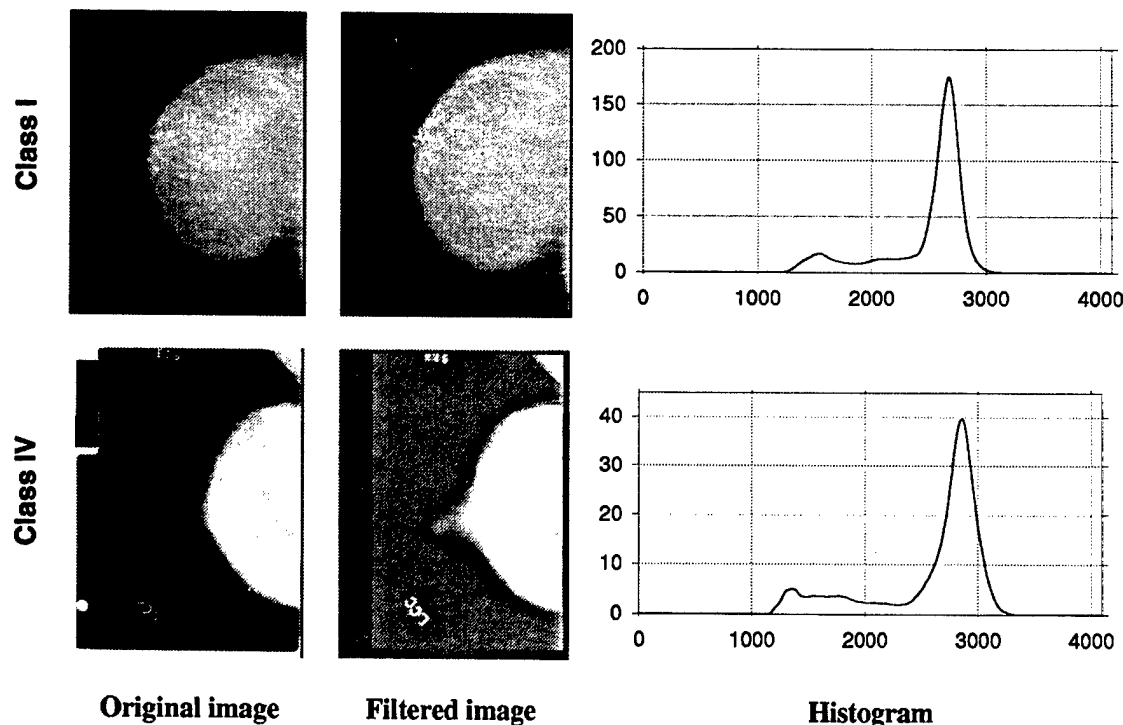


FIG. 9. The gray level histograms of two mammograms classified by radiologists as BI-RADS rating 1 (upper mammogram) and BI-RADS rating 4 (lower mammogram). The shapes of the histograms are very similar and cannot be distinguished by our current histogram analysis method. These two examples were correctly classified with the additional Std and NSH criteria.

necessary to investigate if other classification strategies can be more effective than a rule-based method. Furthermore, we have not performed a systematic study to optimize the many parameters used in the segmentation algorithm. Further work will be required to investigate the dependence of the segmentation accuracy on the various parameters. The parameter selection and the performance of the computer classifier will have to be improved by training with a larger data set and its generalizability evaluated with unknown cases. The generalization of the algorithm to images acquired with other digitizers or direct digital mammography systems will also need to be investigated.

## V. CONCLUSION

We are developing an image analysis method for automated segmentation of the dense area from mammograms and estimation of the percent mammographic density. Our preliminary study indicates the feasibility of our approach. The computer-estimated mammographic breast density correlate closely with the average manual segmentation by five experienced radiologists and the average bias is much less than that of the radiologists' visual estimation. We have found that correct classification of the histogram shapes is the most crucial step in our approach. The histograms of many mammograms have distinctive characteristics that can be recognized by a rule-based classifier. However, some histograms deviate from these rules and this can lead to misclassification. A further investigation will be needed to design more robust rules or classifiers to improve the classification accuracy. Despite these limitations, we have

demonstrated in this preliminary study that the estimation of mammographic density can be performed efficiently and accurately by the automated image analysis tool. The fully automated algorithm can provide an objective and reproducible quantitative estimation of mammographic breast density that is expected to be superior to subjective visual assessment and comparable to manual segmentation by radiologists.

## ACKNOWLEDGMENTS

This work is supported by USPHS Grant No. CA48129, U.S. Army Medical Research and Material Command grants (DAMD 17-99-1-9294) and (DAMD 17-01-1-0326) and by a Career Development Award (B.S) from the USAMRMC (DAMD 17-96-1-6012). The content of this paper does not necessarily reflect the position of the government and no official endorsement of any equipment and product of any companies mentioned in this paper should be inferred.

## APPENDIX A: GRAY-LEVEL THRESHOLDING—DISCRIMINANT ANALYSIS (DA) METHOD

Suppose the probability of the gray level  $n_i$  in an image with  $L$  gray levels can be estimated as

$$p_i = n_i / N, \quad N = \sum_{i=1}^L n_i. \quad (\text{A1})$$

If the pixels in the image are classified into two classes  $C_0$  and  $C_1$  by the threshold  $k$ , then the probabilities of class occurrence and the class mean levels are given by

$$\omega_0 = \sum_{i=1}^k p_i = P(k), \quad \omega_1 = \sum_{i=k+1}^L p_i = 1 - P(k), \quad (\text{A2})$$

$$\mu_0 = \sum_{i=1}^k i p_i / \omega_0 = \mu(k) / \omega_0, \quad (\text{A3})$$

$$\mu_1 = \sum_{i=k+1}^L i p_i / \omega_1 = \frac{\mu_T - \mu(k)}{1 - P(k)},$$

where

$$P(k) = \sum_{i=1}^k p_i, \quad \mu(k) = \sum_{i=1}^k i p_i \quad \text{and} \quad \mu_T = \sum_{i=1}^L i p_i, \quad (\text{A4})$$

are the zeroth- and the first-order cumulative moments of the histogram up to the  $k$ th level, and the total mean level of original image, respectively.

The between-class variance is defined as

$$\sigma_B^2(k) = \omega_0(\mu_0 - \mu_T)^2 + \omega_1(\mu_1 - \mu_T)^2$$

$$= \omega_0 \omega_1 (\mu_1 - \mu_0)^2 = \frac{[\mu_T P(k) - \mu(k)]^2}{P(k)[1 - P(k)]}, \quad (\text{A5})$$

and the optimal threshold  $k^*$  is given by

$$\sigma_B^2(k^*) = \max_{1 \leq k \leq L} \sigma_B^2(k). \quad (\text{A6})$$

## APPENDIX B: GRAY-LEVEL THRESHOLDING—MAXIMUM ENTROPY PRINCIPLE (MEP) METHOD

Suppose the probability of the gray level  $n_i$  in an image with  $L$  gray levels can be estimated as

$$p_i = n_i / N, \quad N = \sum_{i=1}^L n_i. \quad (\text{B1})$$

After thresholding the image by threshold  $k$ , the *a posteriori* probability of the pixels with gray level value less than  $k$ , is given by

$$F(k) = \sum_{i=0}^k p_i. \quad (\text{B2})$$

And the *a posteriori* probability of all those pixels with values greater than or equal to  $k$  is  $1 - F(k)$ . Thus the Shannon entropy of the thresholded image is

$$H(F(k)) = -F(k) \log F(k) - (1 - F(k)) \log(1 - F(k)). \quad (\text{B3})$$

The optimal threshold  $k$  maximizes  $H(F(k))$ .

<sup>a</sup>Correspondence: Heang-Ping Chan, Ph.D., University of Michigan, Department of Radiology, 1500. Medical Center Drive, UHB1F510B, Ann Arbor, Michigan 48109-0030. Electronic mail: chanhp@umich.edu

<sup>1</sup>S. H. Landis, T. Murray, S. Bolden, and P. A. Wingo, "Cancer statistics, 1998," *Ca-Cancer J. Clin.* **48**, 6-29 (1998).

<sup>2</sup>J. N. Wolfe, "Breast patterns as an index of risk for developing breast cancer," *Am. J. Roentgenol.* **126**, 1130-1139 (1976).

<sup>3</sup>J. N. Wolfe, A. F. Saftlas, and M. Salane, "Evaluation of mammographic densities: A case-control study," *Am. J. Roentgenol.* **148**, 1087-1092 (1987).

<sup>4</sup>N. F. Boyd et al., "Mammographic patterns and breast cancer risk: methodologic standards and contradictory results," *J. Natl. Cancer Inst.* **72**, 1253-1259 (1984).

<sup>5</sup>A. F. Saftlas and M. Szklo, "Mammographic parenchymal patterns and breast cancer risk," *Epidemiol. Rev.* **9**, 146-174 (1987).

<sup>6</sup>J. Brisson, R. Verreault, A. S. Morrison, D. Tennina, and F. Meyer, "Diet, mammographic features of breast tissue, and breast cancer risk," *Am. J. Epidemiol.* **130**, 14-24 (1989).

<sup>7</sup>A. F. Saftlas, R. N. Hoover, L. A. Brinton, M. Szklo, D. R. Olson, M. Salane, and J. N. Wolfe, "Mammographic densities and risk of breast cancer," *Cancer (N.Y.)* **67**, 2833-2838 (1991).

<sup>8</sup>A. M. Oza and N. F. Boyd, "Mammographic parenchymal patterns: A marker of breast cancer risk," *Epidemiol. Rev.* **15**, 196-208 (1993).

<sup>9</sup>C. Byne, "Studying mammographic density: Implications for understanding breast cancer," *J. Natl. Cancer Inst.* **89**, 531-532 (1997).

<sup>10</sup>W. Leung, F. Goldberg, B. Zee, and E. Sterns, "Mammographic density in women on postmenopausal hormone replacement therapy," *Surgery (St. Louis)* **122**, 669-674 (1997).

<sup>11</sup>N. F. Boyd, C. Greenberg, G. Lockwood, L. Little, L. Martin, J. Byng, Y. Martin, and D. Trichter, "Effects at two years of a low-fat, highcarbohydrate diet on radiologic features of the breast: Results from a randomized trial," *J. Natl. Cancer Inst.* **89**, 488-467 (1997).

<sup>12</sup>D. V. Spicer, G. Ursin, Y. R. Parisky, J. G. Pearce, D. Shoupe, A. Pike, and M. C. Pike, "Changes in mammographic densities induced by a hormonal contraceptive designed to reduce breast cancer risk," *J. Natl. Cancer Inst.* **86**, 431-436 (1994).

<sup>13</sup>C. Byne, C. Schairer, J. N. Wolfe, N. Parekh, M. Salane, L. A. Brinton, R. Hoover, and R. Haile, "Mammographic features and breast cancer risk: Effects with time, age, and menopause status," *J. Natl. Cancer Inst.* **87**, 1622-1629 (1995).

<sup>14</sup>J. W. Byng, N. F. Boyd, E. Fishell, R. A. Jong, and M. J. Yaffe, "Automated analysis of mammographic densities," *Phys. Med. Biol.* **41**, 909-923 (1996).

<sup>15</sup>S. J. Graham, M. J. Bronskill, J. W. Byng, M. J. Yaffe, and N. F. Boyd, "Quantitative correlation of breast tissue parameters using magnetic resonance and x-ray mammography," *Br. J. Cancer* **73**, 162-168 (1996).

<sup>16</sup>M. J. Yaffe, N. F. Boyd, J. W. Byng, R. A. Jong, R. Fishell, G. A. Lockwood, L. E. Little, and D. L. Trichter, "Breast cancer risk and measured mammographic density," *Eur. J. Cancer Prev.* **7**, S47-S55 (1998).

<sup>17</sup>J. M. Boone, K. K. Lindfors, C. S. Veatty, and J. A. Seibert, "A breast density index for digital mammograms based on radiologists' ranking," *J. Digital Imaging* **11**, 101-115 (1998).

<sup>18</sup>*American College of Radiology. Breast Imaging—Reporting and Data System (BI-RADS)*, 3rd ed. (American College of Radiology, Reston, VA, 1998).

<sup>19</sup>E. White, P. Velentgas, M. T. Mandelson, C. D. Lehman, J. G. Elmore, P. Porter, Y. Yasui, and S. H. Taplin, "Variation in mammographic breast density by time in menstrual cycle among women aged 40-49 years," *J. Natl. Cancer Inst.* **90**, 906-910 (1998).

<sup>20</sup>C. Zhou, H. P. Chan, N. Petrick, B. Sahiner, H. M. A. M. A. Roubidoux, L. M. Hadjiiski, and M. M. Goodsitt, "Computerized image analysis: Estimation of breast density on mammograms," *Proc. SPIE* **3979**, 1615-1624 (2000).

<sup>21</sup>K. E. Martin, M. A. Helvie, C. Zhou, M. A. Roubidoux, J. E. Baily, C. Paramagul, and H. P. Chan, "Automatic computer-aided quantitative assessment of mammographic density: A validation study," *100th Annual Meeting of American Roentgen Ray Society*, Washington, DC, 7-12 May 2000.

<sup>22</sup>A. R. Morton, H. P. Chan, and M. M. Goodsitt, "Automated model-guided breast segmentation algorithm," *Med. Phys.* **23**, 1107-1108 (1996).

<sup>23</sup>M. M. Goodsitt, H. P. Chan, B. Liu, A. R. Morton, S. V. Guru, S. Keshavmurthy, and N. Petrick, "Classification of compressed breast shape for the design of equalization filters in mammography," *Med. Phys.* **25**, 937-948 (1998).

<sup>24</sup>N. Otsu, "A threshold selection method from gray-level histograms," *IEEE Trans. Syst. Man Cybern.* **9**, 62-66 (1979).

<sup>25</sup>A. K. C. Wong, "A gray-level threshold selection method based on

maximum entropy principle," *IEEE Trans. Syst. Man Cybern.* **19**, 866–871 (1989).

<sup>26</sup>J. N. Kapur, "Twenty-five years of maximum-entropy principle," *J. Math. Phys.* **17**, 103–156 (1983).

<sup>27</sup>K. E. Martin, M. A. Helvic, C. Zhou, M. A. Roubidoux, J. Bailey, P. C., C. Blanc, K. Klein, S. Sonnad, and H. P. Chan, "Mammographic density measured by an automatic computer-aided quantitative method: a feasibility study," *Am. J. Roentgenol.* (submitted).

# Breast Density Estimation: Correlation of Mammographic Density and MR Volumetric Density



Heang-Ping Chan, Lubomir M. Hadjiiski, Marilyn A. Roubidoux, Mark A. Helvie,  
Sophie Paquerault, Berkman Sahiner, Jun Wei,  
Chuan Zhou, Thomas Chenevert, Mitchell M. Goodsitt

Department of Radiology, The University of Michigan, Ann Arbor, Michigan 48105, USA

## ABSTRACT

Studies have demonstrated a strong correlation between mammographic breast density and breast cancer risk. Mammographic breast density may therefore be used as a surrogate marker for monitoring the response to treatment in studies of breast cancer prevention or intervention methods.

In this study, we evaluated the accuracy of using mammograms for estimating breast density by analyzing the correlation between the percent mammographic dense area and the percent fibroglandular tissue volume obtained from MR images. A data set of 37 patients who had corresponding MR images and mammograms was collected. The fibroglandular tissue regions in the MR slices were segmented by a semi-automatic method and the percent fibroglandular tissue volume calculated. Mammographic breast density was estimated by an automated image analysis program—Mammographic Density ESTimator (MDEST) that we developed previously. It was found that the correlation between the percent dense area of the CC and MLO views and the percent fibroglandular tissue volume on MR images was 0.93 and 0.91, respectively, with a mean bias of 4.4%. The high correlation indicates the usefulness of mammographic density as a surrogate for breast density estimation.

## MATERIALS AND METHODS

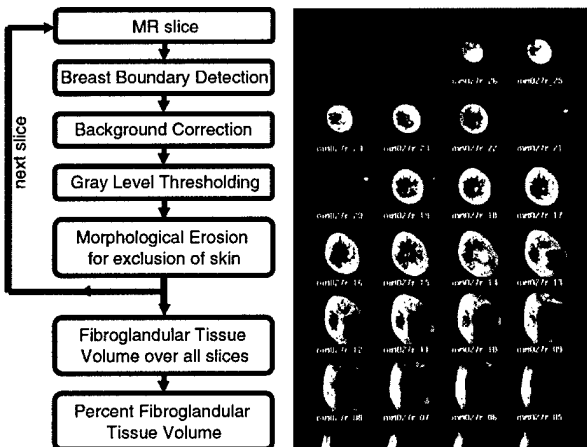
### DATA SET

37 patients, corresponding MR breast images and mammograms:

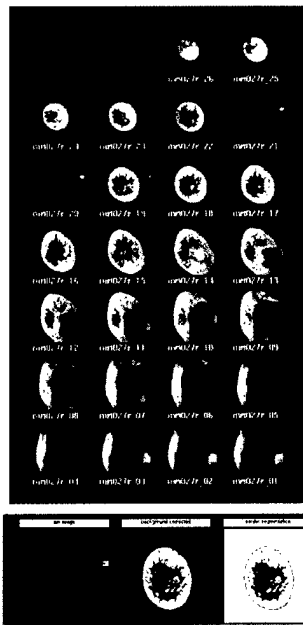
MR series: Coronal 3D T1-weighted pre-contrast images  
3D Spoiled Gradient-Recalled Echo (SPGR)  
TE=3.3 ms; TR=10 ms, Flip=40 deg, matrix=256x128,  
FOV=28-32 cm right/left, 14-16 cm superior/inferior,  
scan time=2 min 38 sec  
Coronal sections 2-5 mm thick, 32 slices;  
Full volume coverage of both breasts with contiguous slices

Mammograms: GE DMR mammography system (Mo/Mo, Mo/Rh, Rh/Rh)  
CC and MLO views

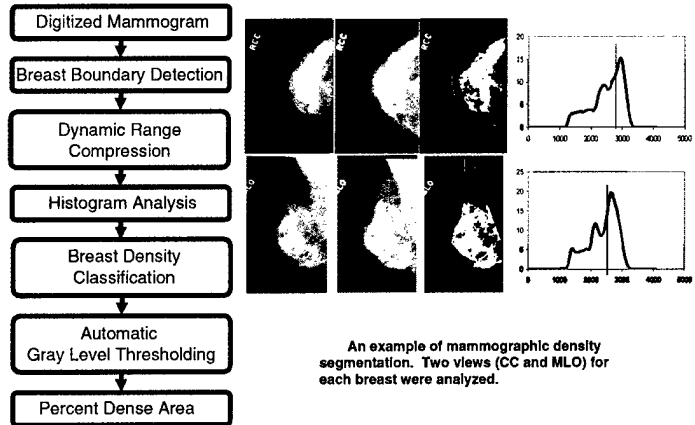
## MR BREAST IMAGE SEGMENTATION



Example of MR images from one breast. Although the MR pulse sequence is not the optimal one for separating water and fat, the fibroglandular parenchyma (~water) and fatty tissue are well separated with this heavily T1-weighted acquisition. Breast boundaries were automatically detected and then manually corrected if necessary.

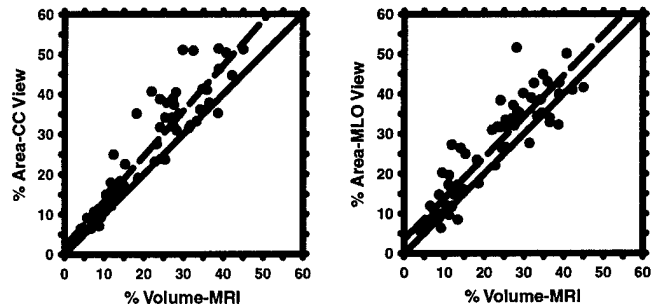


## MAMMOGRAM SEGMENTATION



An example of mammographic density segmentation. Two views (CC and MLO) for each breast were analyzed.

## RESULTS



| Mammographic View                         | CC   | MLO  |
|---|------|------|
| Correlation Coefficient                   | 0.93 | 0.91 |
| Root-mean-square residual                 | 5.2  | 5.3  |
| Mean difference between %Area and %Volume | 4.7  | 4.1  |

## CONCLUSION

Although the % projected area and the % volume of fibroglandular tissue in the breast are not expected to be linearly related, the correlation between the two estimates was found to be very high. This result indicates the usefulness of mammographic density as a surrogate of % fibroglandular tissue volume for study of the correlation between breast density and breast cancer risk. The computerized image analysis tool (MDEST) is useful for estimation of mammographic density. The automated analysis is expected to contribute to the understanding of the relationship of mammographic density to breast cancer risk, detection, and prognosis, and to the prevention and treatment of breast cancer.

## ACKNOWLEDGMENTS

This work is supported by U. S. Army Medical Research and Materiel Command grants DAMD 17-01-1-0326 and DAMD 17-99-1-9294. The content of this paper does not necessarily reflect the position of the government and no official endorsement of any equipment and product of any companies mentioned should be inferred.

## **Breast Density Estimation: Correlation of Mammographic Density and MR Volumetric Density**

Heang-Ping Chan, Lubomir M. Hadjiiski, Marilyn A. Roubidoux, Mark A. Helvie,  
Sophie Paquerault, Berkman Sahiner, Jun Wei, Chuan Zhou,  
Thomas Chenevert, Mitchell M. Goodsitt

Department of Radiology, University of Michigan, Ann Arbor, MI 48109  
Chanhp@umich.edu

**Abstract.** Studies have demonstrated a strong correlation between mammographic breast density and breast cancer risk. Mammographic breast density may therefore be used as a surrogate marker for monitoring the response to treatment in studies of breast cancer prevention or intervention methods. In this study, we evaluated the accuracy of using mammograms for estimating breast density by analyzing the correlation between the percent mammographic dense area and the percent glandular tissue volume as estimated from MR images. A data set of 37 patients who had corresponding MR images and mammograms was collected. The glandular tissue regions in the MR slices were segmented by a semi-automatic method and the percent glandular tissue volume calculated. Mammographic breast density was estimated by an automated image analysis program. It was found that the correlation between the percent dense area of the CC and MLO views and the percent volumetric fibroglandular tissue on MR images was 0.93 and 0.91, respectively, with a mean bias of 4.4%. The high correlation indicates the usefulness of mammographic density as a surrogate for breast density estimation.

### **1. Introduction**

Previous studies have shown that there is a strong positive correlation between breast parenchymal density on mammograms and breast cancer risk [1-3]. The relative risk is estimated to be about 4 to 6 times higher for women whose mammograms have parenchymal densities over 60% of the breast area, as compared to women with less than 5% of parenchymal densities. The change in mammographic breast density is therefore often used as an indicator for monitoring the effects of preventive or interventional treatment of breast cancer.

Breast cancer risk is expected to depend on the volume of glandular tissue in the breast. Mammographic density is a projection of the volume of glandular tissue onto the two-dimensional image plane. To better understand the correlation between mammographic density and breast cancer risk, it is important to investigate the relationship between the projected areal density on mammograms and the volume of glandular tissue in the breast. In this study, we investigate this relationship by analyzing the percent volumetric glandular tissue in magnetic resonance (MR) images and the percent dense area in corresponding mammograms for the same breasts.

## 2. Materials and Methods

Our data set consisted of corresponding MR breast images and mammograms from 37 patients acquired between detection and biopsy. The MR image series used in this study, which included coronal 3D T<sub>1</sub>-weighted pre-contrast images (coronal sections 2-5 mm thick, 32 slices; 3D Spoiled Gradient-Recalled Echo (SPGR); TE=3.3ms; TR=10ms, Flip=40°, matrix=256x128, FOV=28-32cm right/left, 14-16cm superior/inferior, scan time=2 min 38 sec) was part of a dynamic breast MRI study. This 3D SPGR sequence produced full volume coverage of both breasts with contiguous image slices. An example of images from one breast is shown in Fig. 1. Although this is not the optimal pulse sequence for separating water and fat, the fibroglandular parenchyma (~water) and fatty tissue are well separated with this heavily T<sub>1</sub>-weighted acquisition and therefore the series was chosen for this study.

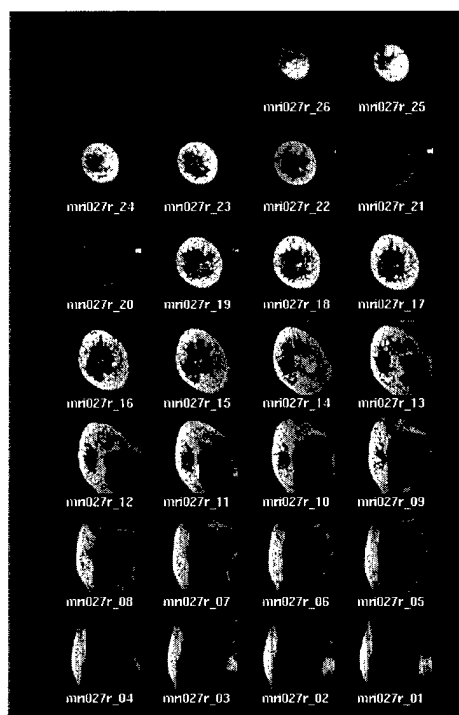


Fig. 1. MR images of the right breast of a patient. The two-view mammogram of the same breast is shown in Fig. 2.

We have developed a graphical user interface that displays the MR series and the corresponding mammogram of each breast. The interface allows the user to perform a combination of manual and automatic operations to segment the MR images. Each MR slice is first thresholded to separate the breast from the surrounding region. For slices close to the chest wall where no clear boundary can be seen, the boundary is manually drawn and evaluated by radiologists. Background correction [4] using the voxel values around the segmented breast region is employed to correct for the non-

uniformity across the breast area due to the breast coil. The histogram of the voxel values in the breast region is then formed and interactive thresholding is used to segment the fibroglandular tissue from the fatty tissue. A morphological erosion operation along the breast boundary then excludes the skin voxels from the calculation of the fibroglandular tissue area in each slice. Finally, an integration of the fibroglandular voxels in all slices relative to the breast volume provides the percent volumetric fibroglandular tissue in the breast.

We have previously developed an automated image analysis tool (Mammographic Density ESTimator) to assist radiologists in estimating mammographic breast density [5]. MDEST performs dynamic range compression, breast boundary tracking, pectoral muscle segmentation for the MLO view, automatic thresholding based on gray level histogram analysis, and calculates the percent dense area on a mammogram. We found that the correlation between the computer-estimated percent dense area and radiologists' manual segmentation was 0.94 and 0.91, respectively, for CC and MLO views, with a mean bias of less than 2%. An example of a mammogram segmented by MDEST is shown in Fig. 2.

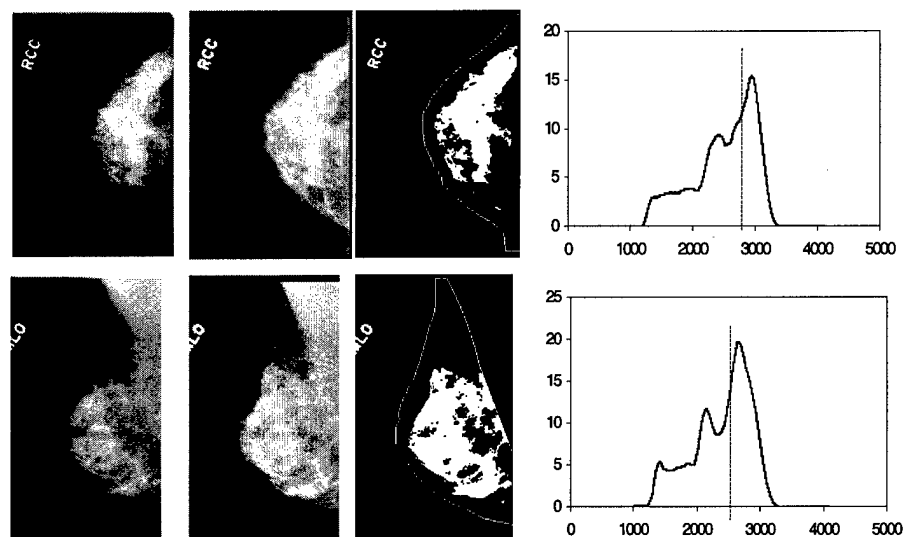


Fig. 2. Automated breast density segmentation from mammograms. Upper row: CC view. Lower row: MLO view.

### 3. Results

Scatter plots of the percent volumetric fibroglandular tissue versus the percent dense area on mammograms are shown in Fig. 3(a) and 3(b) for the CC- and MLO-view mammograms, respectively. The correlation of percent dense area of the CC and MLO views with the percent volumetric fibroglandular tissue on MR images was found to be 0.93 and 0.91, respectively, with a mean bias of 4.4%.

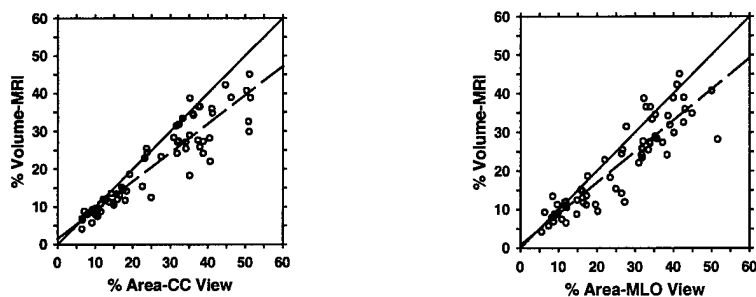


Fig. 3. Correlation of % volumetric fibroglandular tissue on MR images with % dense area on mammograms for 37 patients. The left and right breasts are plotted as separate data points on each graph. The dash lines are linear least squares fits to the data points.

#### 4. Conclusion

Mammographic density is highly correlated with the volumetric fibroglandular tissue in the breast, indicating its usefulness as a surrogate for breast density estimation. The computerized image analysis tool, MDEST, is useful for estimation of mammographic density. The automated analysis is expected to contribute to the understanding of the relationship of mammographic density to breast cancer risk, detection, and prognosis, and to the prevention and treatment of breast cancer.

#### Acknowledgements

This work is supported by U. S. Army Medical Research and Materiel Command grants DAMD 17-01-1-0326 and DAMD 17-99-1-9294. The content of this paper does not necessarily reflect the position of the government and no official endorsement of any equipment and product of any companies mentioned should be inferred.

#### References

1. J. Brisson, R. Verreault, A. S. Morrison, D. Tennina and F. Meyer, "Diet, mammographic features of breast tissue, and breast cancer risk," *Am. J. Epidemiology* 130, 14-24 (1989).
2. A. F. Saftlas, R. N. Hoover, L. A. Brinton, M. Szklo, D. R. Olson, M. Salane and J. N. Wolfe, "Mammographic densities and risk of breast cancer," *Cancer* 67, 2833-2838 (1991).
3. N. F. Boyd, G. A. Lockwood, J. W. Byng, D. L. Tritchler and M. J. Yaffe, "Mammographic densities and breast cancer risk," *Cancer Epidemiology Biomarkers & Prevention* 7, 1133-1144 (1998).
4. B. Sahiner, H. P. Chan, N. Petrick, D. Wei, M. A. Helvie, D. D. Adler and M. M. Goodsitt, "Classification of mass and normal breast tissue: A convolution neural network classifier with spatial domain and texture images," *IEEE Trans Med Imag* 15, 598-610 (1996).
5. C. Zhou, H. P. Chan, N. Petrick, M. A. Helvie, M. M. Goodsitt, B. Sahiner and L. M. Hadjiiski, "Computerized image analysis: Estimation of breast density on mammograms," *Med Phys* 28, 1056-1069 (2001).